

Correlations and Simulations in Polymer Science

Many properties of polymers can be easily measured by use of relatively simple instrumentation as discussed in earlier chapters. Standardized testing methods have been formulated by the American Society of Testing Methods (ASTM). A partial listing of these standards for plastics and rubber is given in Appendix C. When a polymer has not yet been synthesized or perhaps is unavailable or in quantities too small to fully test, a variety of approaches can be used to accurately *predict* polymer properties. In addition, these methods can be used to investigate how systematic structural changes such as the substitution of different chemical groups may affect polymer properties. Early approaches include group-contribution methods that have been successfully used to predict the properties of small molecules [1]. This approach has been adapted for polymers by van Krevelen [2, 3] whereby the repeat unit is divided into individual atoms or small chemical groups such as methyl or

phenyl groups that contribute incrementally to a specific property. Another successful approach for predicting polymer properties makes use of topological and geometrical parameters [4]. This approach offers a reliable alternative method to group-contribution methods and is particularly valuable in cases when specific chemical groups are unavailable in more traditional group-contribution methods. In some cases, artificial neural networks (ANNs) have been used to predict properties or to optimize processing operations using a set of descriptors and a large (training) set of experimental data. A fourth approach is the use of molecular simulations that can provide information on physical, mechanical, and transport properties. The accuracy of simulations depends upon the quality of a molecular mechanics force field that describes the potential-energy surface of the atomistic system. A successful polymer force field requires extensive parameterization for a large number of molecules using experimental data for validation and is applicable for a wide variety of polymers. Each of these approaches is described in the sections that follow.

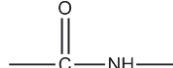
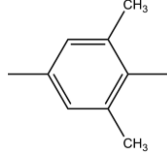
13.1 Group-Contribution Methods

As mentioned in the previous paragraph, an extensive collection of group-contribution methods for estimating polymer properties has been given by van Krevelen [2, 3]. Important applications of group-contribution methods include predictions of mechanical properties, surface energy, viscosity, density, thermal expansion coefficient, heat capacity, glass-transition temperature, crystalline-melt temperature, permeability, solubility parameters, free volume, and chemical potential. In this section, only a few of the more common group-contribution methods are illustrated. For more extensive treatment of group-contribution methods including comparisons of experimental and predicted properties, refer to the treatise by van Krevelen [2] and other sources.

13.1.1 Volumetric Properties

An important physical property that can be obtained by group contributions is specific or molar volume that provides an estimation of polymer density. As shown by selected values in Table 13-1, group-contribution increments are available to calculate specific volumes of glassy, rubber, and crystalline states at 298 K and consequently density as illustrated in Example 13.1. Group-contribution methods given by van Krevelen also can be used to calculate the van der Waals volume of a polymer, from which the fractional free volume can be obtained as shown in Example 13.2.

Table 13-1 Representative van Krevelen [2] Values for Molar Volume Increments (Bivalent Groups) at 298 K

Group	$V_{a,i}^a$ (cm ³ /mol)	$V_{c,i}^a$ (cm ³ /mol)	V_w (cm ³ /mol)
—CH ₂ —	16.37	14.68	10.23
—CF ₂ —	23.7	21	14.8
—C(CH ₃) ₂ —	49.0	44.0	30.7
—Si(CH ₃) ₂ —	67.5	60.6	42.2
—CH(CH ₃)—	32.72	29.35	20.45
—CH(CN)—	30.7	27.5	21.5
—CH(C ₆ H ₅)—	84.16	75.48	52.6
—CH=CH—	27.0	24.3	16.9
—CH=CCl—	41.0	37.0	25.7
—CH=C(CH ₃)—	<i>cis</i> 43 <i>trans</i> 43	40 37	27.2
—O—	al ^b (8.5) ar ^b (8.0)	(7.9) (7.1)	(5.5) (5.0)
	(21)	(18.7)	18.9 (13)
—COO—	gen ^c 23 acr ^c 20.5	21.5 18.4	15.2
—OCOO—	31	27	18.9
	65.5	59	43.3
	104	94	65.6

^a Subscripts a and c on $V_{a,i}$, and $V_{c,i}$ correspond to the fully amorphous and fully crystalline states, respectively; V_w is the van der Waals molar volume.

^b *al*, aliphatic oxygen; *ar*, aromatic oxygen.

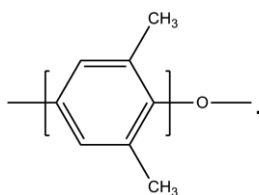
^c *gen*, general; *acr*, acrylic.

Example 13.1

Calculate the specific density of poly(2,6-dimethyl-1,4-phenylene oxide) using group-contribution methods.

Solution

The repeating unit of poly(2,6-dimethyl-1,4-phenylene oxide) is



Poly(2,6-dimethyl-1,4-phenylene oxide) is an *amorphous* polymer with a T_g of 214°C (see Section 10.1.4). The molecular weight of the repeating unit is $8(12.011) + 15.994 + 8(1.00794) = 120.151$. Using values from Table 13-1, the molar volume is calculated to be $104 + 8.0 = 112.0 \text{ cm}^3/\text{mol}$. Specific volume is then calculated as

$$V_a = 112 \frac{\text{cm}^3}{\text{mol}} \frac{\text{mol}}{120.2 \text{ g}} = 0.9318 \frac{\text{cm}^3}{\text{g}}.$$

Specific density is then calculated as $1/0.9318 = 1.073 \text{ g/cm}^3$. This value is in excellent agreement with a reported experimental value of 1.06 g/cm^3 at 296 K [5].

Van der Waals Volume. The van der Waals volume, V_w , of a molecule is the atomistic space occupied by the molecule. Values for selected van der Waals volume increments are included in Table 13-1 for bivalent groups (i.e., two valence connection sites) and in Table 13-2 for non-bivalent groups (one, three, or four valence connection sites). An important use of V_w is the estimation of *fractional free volume* (FFV) defined as

$$\text{FFV} = \frac{V - V_o}{V} \quad (13.1)$$

where V is the specific volume of the polymer at a given temperature and V_o is the volume occupied by the polymer chains. The FFV directly relates to important polymer properties such as viscosity and diffusivity or permeability as given by the equation

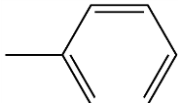
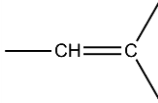
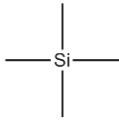
$$P = A \exp\left(\frac{-B}{\text{FFV}}\right). \quad (13.2)$$

Bondi [6] has suggested that an occupied “volume,” V_o , can be obtained from the van der Waals volume of the various groups comprising the polymer repeat unit as

$$V_o = 1.3 \sum_{k=1}^N (V_w)_k \quad (13.3)$$

where N is the total number of groups in the repeat unit.

Table 13-2 Representative van Krevelen [2] Values for van der Waals Volume Increments (non-Bivalent Groups) at 298 K

Group	V_w^a (cm ³ /mol)
—H	3.44
—CH ₃	27.2
—C≡N	14.7
—OH	8.0
—F	5.7
—Cl	al 11.6 ar 12.0
	45.85
—C≡	(8)
	13.5
	16.6

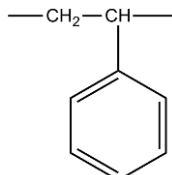
^a *al*, aliphatic oxygen; *ar*, aromatic oxygen.

Example 13.2

Calculate the fractional free volume (FFV) of atactic polystyrene (aPS) using only group contributions.

Solution

The repeating unit of PS is



Group Contribution	V_a	V_w
—CH ₂ —	16.37	10.23
—CH(C ₆ H ₅)—	84.16	52.6

The molar volume, V , of α -PS is obtained by summing the group contributions of V_a taken from Table 13-1 as 100.53 (16.37 + 84.16) cm³/mol. Similarly, the van der

Waals volume obtained by summing the group contributions, V_w (Table 13-1), is 62.83 cm³/mol (10.23 + 52.6). The occupied volume is then obtained from eq. (13.3) as $V_o = 1.3 \times 62.8 = 81.7$ cm³/mol. Finally, the FFV is obtained from eq. (13.1) as

$$\text{FFV} = \frac{V - V_o}{V} = \frac{100.5 - 81.7}{100.5} = \frac{18.8}{100.5} = 0.187.$$

This value compares favorably with a value of 0.177 reported by Thran et al. [7].

13.1.2 Glass-Transition Temperature

Correlations to predict the glass-transition temperature (T_g) have been reviewed by Fried [8]. Van Krevelen [2] has summarized some early approaches. A simple correlation used by van Krevelen for T_g is given as

$$T_g = \frac{\sum_i Y_{g,i}}{M} = \frac{Y_g}{M} \quad (13.4)$$

where Y_g is the molar glass-transition function (units of K·kg/mol), $T_{g,i}$, and M is the molecular weight (kg/mol) of the structural unit. In evaluation of a set of nearly 600 polymers, it was observed that Y_g depends upon the nature of other groups present in the structural unit and, therefore, correction terms must be added in the numerator for different functional groups. A plot of predicted versus experimental T_g values for 55 vinyl and aromatic-backbone polymers over the temperature range from about 200 to 441 K is shown in Figure 13-1. Agreement for this group of polymers is quite satisfactory ($R^2 = 0.8177$). The calculation of the T_g of bisphenol-A polycarbonate from group contribution is shown next in Example 13.3.

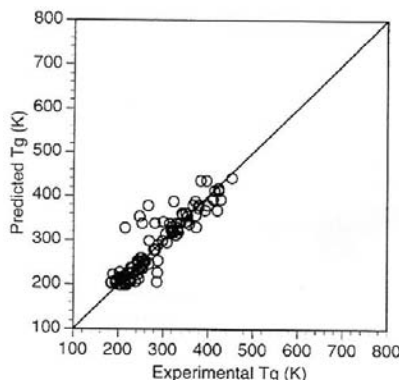
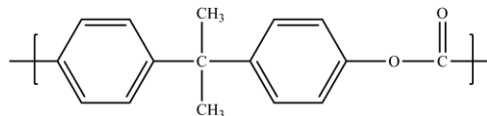


Figure 13-1 Plot of predicted (eq. (13.4)) versus experimental T_g of 55 polymers reported by van Krevelen [2].

Example 13.3

Calculate the T_g of bisphenol-A polycarbonate (PC) using van Krevelen's parameters. The repeating unit structure of PC is shown below.



Solution

The selected structural groups for PC and their corresponding molecular weights and molar glass-transition functions (van Krevelen [2] parameters) are shown in the table below.

Group	$Y_{g,i}^a$	M_i
	20	60.0
	87	194.3
	$\sum =$	107 254.3

^a Units of $Y_{g,i}$ are K·kg/mol.

The molecular weight of the repeating unit is then calculated as $60.0 + 194.3 = 254.3$ and the corresponding sum of the molar glass-transition functions is 107. The T_g is then calculated from eq. (13.4) as

$$T_g = \frac{\sum_i Y_{g,i}}{M} = \frac{107 \text{ K kg/mol}}{254.3 \text{ kg/kmol}} \times \frac{1000 \text{ mol}}{\text{kmol}} = 421 \text{ K.}$$

This value compares favorably with reported experimental values [5] ranging from 413 to 424 K.

13.1.3 Permeability

The permeability of glassy and rubbery polymers has been discussed in Section 12.1.2. Several approaches have been proposed to predict polymer permeability from chemical group contributions. For example, Salame [9, 10] has proposed that gas permeability, particularly for low-permeability (i.e., barrier) polymers, can be

predicted from the value of the polymer Permachor, π , calculated from the relationship

$$\pi = \frac{1}{N} \sum_i (N_i \cdot \Pi_i) \quad (13.5)$$

where N is the total number of characteristic groups per structural unit, N_i is the number of i groups in the structural unit, and Π_i is the increment of group i contributing to the Permachor. Representative values of incremental Permachor values are given in Table 13-3.

Once the Permachor is calculated from the structure, the permeability at 298 K, $P(298)$, for nitrogen and other gases is then obtained from the equation

$$P(298) = P^*(298) \exp(-s\pi) \quad (13.6)$$

where $P^*(298)$ is the permeability (in SI units of $\text{cm}^3(\text{STP}) \text{ cm}/\text{cm}^2\text{-s-Pa}$)^{*} of the gas in natural rubber and s is a scaling factor ($s = 0.12$ for O_2 , N_2 , and CO_2). In the case of nitrogen, $\log P^*(298)$ is -12. Once the permeability for nitrogen has been calculated, permeabilities of O_2 and CO_2 can be approximated by relative permeabilities averaged for many polymers using nitrogen as the standard gas (e.g., $P(\text{N}_2):P(\text{O}_2):P(\text{CO}_2)::1:3.8:24$). Although Permachor values are valid only for amorphous polymers, corrections are available to account for crystallinity [2]. As shown in Figure 13-2, there is excellent agreement between experimental permeability values for O_2 , N_2 , and CO_2 and permeabilities predicted from Permachor values. Example 13.4 illustrates the use of the Permachor approach to predict the oxygen permeability of polydimethylsiloxane. It is important to recognize that the extent of success for the Permachor method, like other group-contribution methods such as that for estimating T_g or the solubility parameter as shown in the following section, is limited by the availability of group contributions for structural units of less common but still important engineering and specialty polymers such as polyimides and polyphosphazenes (see Section 10.2.5) that have hundreds of possible chemical variations. Several alternative approaches for permeability prediction are available [2, 4].

* The unit $\text{cm}^3(\text{STP})$ is the amount of gas in units of cm^3 at standard temperature and pressure (i.e., 273 K, 1 bar).

Table 13-3 Selected Group Contributions to the Molar Permachor^a

Group	Π_i
—CH ₂ —	15
—CF ₂ —	120
—CH(CH ₃)—	15
—CH(CN)—	205
—C(CH ₃) ₂ —	-20
—Si(CH ₃) ₂ —	-116
-CH(<i>i</i> -butyl)-	-1
—CH=CH—	-12
—CH=CCl—	33
—CH=C(CH ₃)—	-30
—O—	70
O	309
—C—NH—	(wet 210)

^a Values taken from Salame [10].

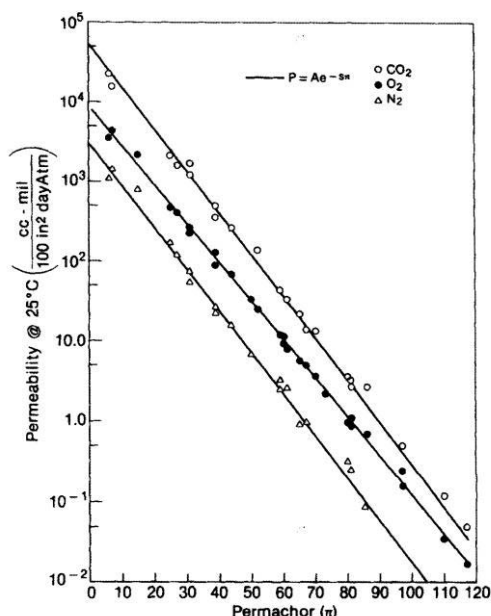
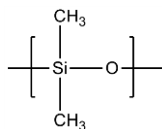


Figure 13-2 Correlation of gas permeability to polymer Permachor. Experimental data are given for oxygen (●), nitrogen (Δ), and carbon dioxide (○). Reproduced from M. Salame, *Prediction of Gas Barrier Properties of High Polymers*. Polymer Engineering and Science, 1986. **26**(22): p. 1543–1546. Reprinted by permission of John Wiley & Sons, Inc.

Example 13.4

Calculate the oxygen permeability of polydimethylsiloxane (PDMS)



using the molar Permachor values listed in Table 13-3.

Solution

The Permachor is calculated using eq. (13.5) as

$$\pi = \frac{1}{2} [(1)(-116) + (1)(70)] = -23.$$

Next the nitrogen permeability is obtained from eq. (13.6) as

$$P(298) = (10^{-12}) \exp [(-0.12)(-23)] = 1.58 \times 10^{-11} \text{ cm(STP)} \text{ cm/cm}^2 \text{-s-Pa.}$$

Finally, oxygen permeability is obtained from the relative permeability of O₂ to N₂ (a factor of 3.8), giving the following permeability value:

$$P(298) = 3.8 \times 1.58 \times 10^{-11} = 6.0 \times 10^{-11} \text{ cm(STP)} \text{ cm/cm}^2 \text{-s-Pa.}$$

An experimental value of the oxygen permeability of PDMS at 308 K is reported as $9.33 \times 10^{-8} \text{ cm}^3(\text{STP}) \text{ cm/s cm}^2 \text{ cmHg}$ [11]. Conversion of pressure units from cmHg to Pa (Appendix D, Table D-2) results in a $P(298)$ value of $7.00 \times 10^{-11} \text{ cm}^3(\text{STP}) \text{ cm/cm}^2 \text{s-Pa}$, in good agreement with the experimental value of $6.0 \times 10^{-11} \text{ cm}^3(\text{STP}) \text{ cm/cm}^2 \text{s-Pa}$ cited above.

13.1.4 Solubility Parameter

The concept of the solubility parameter was introduced in Section 3.2.6. Solubility parameters of polymers can be estimated by use of one of several group-contribution methods, such as those given by Small [12] and by Hoy [13]. Calculation of δ by a group-contribution method requires the value of a molar attraction constant, F_i , for each chemical group in the polymer repeat unit. Values of F_i have been obtained by regression analysis of physical property data for a large number of organic compounds (e.g., 640 compounds in Hoy's method). In the case of Small's method, all compounds for which hydrogen bonding occurs (e.g., hydroxyl compounds, amines, and carboxylic acids) were excluded. A listing of some important molar attraction constants is given in Table 13-4.

Table 13-4 Molar Attraction Constants at 25°C

Group	Molar Attraction Constant, F ((MPa) $^{1/2}$ cm 3 mol $^{-1}$)		
	Small [12]	Hoy [13]	Van Krevelen [2]
-CH ₃	438	303	420
-CH ₂ -	272	269	280
>CH-	57	176	140
>C<	-190	65.5	0
-CH(CH ₃)-	495	(479)	560
-C(CH ₃) ₂ -	686	(672)	840
-CH=CH-	454	497	444
>C=CH-	266	422	304
Phenyl	1504	1398	1517
<i>p</i> -Phenylenne	1346	1442	1377
-O- (ether)	143	235	256
-OH	—	462	754
-CO- (ketone)	563	538	685
-COO- (ester)	634	668	512
-OCOO- (carbonate)	—	(904)	767
-CN	839	726	982
-N=C=O	—	734	—
-NH-	—	368	—
-S- (sulfide)	460	428	460
-F	(250)	84.5	164
-Cl (primary)	552	420	471
-Br (primary)	696	528	614
-CF ₃ (<i>n</i> -fluorocarbon)	561	—	—
-Si-	-77	—	—

The solubility parameter of a polymer can then be calculated from the molar attraction constants and the molar volume of the polymer, V (units of cm 3 mol $^{-1}$), from the relationship

$$\delta = \frac{\sum_{i=1} F_i}{V} \quad (13.7)$$

where the summation is taken over all groups in the repeating unit. As shown earlier (Section 13.1.1), the molar volume can be obtained from group contributions as well. Chemical groups can be atoms, particularly halogens or small uniquely identifiable groups in the polymer repeating unit such as methyl, methylene, and phenyl groups as shown in Table 13-4. Calculated values of solubility parameters for some

common solvents and polymers have been tabulated in a number of publications [2, 14, 15]. Some representative values are given in Table 13-5. A sample calculation using Small's method is given next in Example 13.5.

Table 13-5 Solubility Parameters of Some Common Solvents and Polymers

Solvents	Solubility Parameter, δ^a	
	$(\text{MPa})^{1/2}$	$(\text{cal cm}^{-3})^{1/2}$
<i>n</i> -Hexane	14.9	7.28
Carbon tetrachloride	17.8	8.70
Toluene	18.2	8.90
Benzene	18.6	9.09
Chloroform	19.0	9.29
Tetrahydrofuran	19.4	9.48
Chlorobenzene	19.6	9.58
Methylene chloride	20.3	9.92
1,4-Dioxane	20.5	10.0
<i>N</i> -Methyl-2-pyrrolidone	22.9	11.2
Dimethylformamide	24.8	12.1
Methanol	29.7	14.5
Water	47.9	23.4
Polymers		
Polyisobutylene	15.5	7.58
Polysulfone	20.3	9.92
Poly(vinyl chloride)	21.5	10.5
Polystyrene	22.5	11.0
Poly(methyl methacrylate)	22.7	11.1
Cellulose acetate	25.1	12.3
Polyacrylonitrile	25.3	12.4
Poly(vinyl acetate)	25.7	12.7

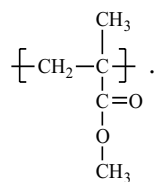
^aCalculated from Hansen solubility parameters using eq. (13.7) at 25°C; conversion: 1 MPa^{1/2} = 0.489 (cal cm³)^{1/2}.

Example 13.5

Estimate the solubility parameters, in units of $(\text{MPa})^{1/2}$, for poly(methyl methacrylate) (PMMA) by the method of Small [12]. The density of PMMA is reported to be 1.188 g cm⁻³ at 25°C.

Solution

The structure of the PMMA repeat unit is



From the available chemical groups listed in Table 13-4, the molar-attraction constant for the repeating unit of PMMA can be obtained as follows:

Group	F	Number of Groups	$\sum F_i$
-CH ₃	438	2	876
-CH ₂ -	272	1	272
>C<	-190	1	-190
-COO- (ester)	634	1	<u>634</u>
			1592

The formula weight of a PMMA repeating unit is calculated from atomic weights (Appendix F) as follows:

$$\begin{array}{lll} \text{C: } & 5 \times 12.01115 & = 60.06 \\ \text{O: } & 2 \times 15.9994 & = 32.0 \\ \text{H: } & 8 \times 1.00797 & = \frac{8.06}{100.12} \end{array}$$

Using the density of PMMA given in the problem statement, the molar volume, V , is then calculated as

$$\frac{200.12}{1.188} = 84.28 \text{ cm}^3 \text{ mol}^{-1}.$$

The solubility parameter is then calculated as

$$\delta_i = \frac{\sum F_i}{V_i} = \frac{1592}{84.28} = 18.9 \text{ MPa}^{1/2}.$$

This value is within about 17% of the value of 22.7 MPa^{1/2} given in Table 13-5 for PMMA. Recalculation of the solubility parameter using Hoy's and van Krevelen's group contributions given in Table 13-4 gives values of 19.1 and 19.4 MPa^{1/2}, respectively, which are a little closer to the reported experimental value.

13.1.5 Activity Coefficients

As discussed in Chapter 3, once a value for the interaction parameter is known or can be estimated, the activity of a solvent in a polymer solution can be estimated by means of the Flory–Huggins equation. It is also possible to *predict* activity through a variety of chemical group-contribution methods [16]. The most fully developed of these methods is UNIFAC-FV [17]. The acronym UNIFAC stands for *UNIQUAC Functional-group Activity Coefficients*, which had been widely used for the prediction of vapor–liquid equilibrium (VLE) for mixtures of low-molecular-weight components [18], and FV represents a free-volume contribution originating from the Flory equation-of-state theory (see Section 3.2.3). UNIQUAC, itself, is an acronym for *Universal Quasi-Chemical equations*, which provides good representation of both vapor–liquid equilibrium (VLE) and liquid–liquid equilibrium (LLE) for binary and multicomponent mixtures of nonelectrolytes using one or two adjustable (energy) parameters per binary pair [19]. The difference between UNIQUAC and UNIFAC, or UNIFAC-FV, is that UNIFAC uses the solution-of-functional-groups (SOG) concept [20] to obtain group-contribution parameters (the adjustable parameters in UNIQUAC) from knowledge of the chemical groups comprising the mixture components in a manner similar to the way that solubility parameters are calculated by the methods of Small or Hoy as discussed in the previous section.

In the UNIFAC-FV approach, solvent activities may be calculated as contributions from three sources—a combinatorial (entropy) term, a residual (enthalpic) term, and a (Flory equation-of-state^{*}) free-volume term as

$$\ln \alpha_1 = \ln \alpha_1^C + \ln \alpha_1^R + \ln \alpha_1^{FV}. \quad (13.8)$$

The combinatorial term is given as

$$\ln \alpha_1^C \approx \ln \phi_1' + \left(1 - \phi_1'\right) + \frac{z}{2} M_1 q_1' \left[\ln \left(\frac{\theta_1'}{\phi_1'} \right) - 1 + \frac{\phi_1'}{\theta_1'} \right] \quad (13.9)$$

where ϕ_1' is the segment volume fraction, θ_1' is the surface area fraction, z is the coordination number of the lattice (taken to be 10), and M_1 is the molecular weight of component 1 (i.e., the solvent in a polymer solution). The parameter q_1' in eq. (13.9) is related to the van der Waals surface area as

$$q_1' = \frac{1}{M_1} \sum_{k=1}^N v_k^{(1)} Q_k \quad (13.10)$$

^{*} See Chapter 3, Section 3.2.3.

where $v_k^{(1)}$ is the number of functional groups of type k in the solvent and Q_k is a group area parameter obtained from the (Bondi) van der Waals group surface area, A_{wk} , and normalized to a methylene unit of polyethylene as

$$Q_k = \frac{A_{wk}}{2.5 \times 10^9}. \quad (13.11)$$

The surface area fraction, θ_1' , is calculated from q_1' as

$$\theta_1' = \frac{q_1' w_1}{\sum_{j=1}^N q_j' w_j} \quad (13.12)$$

where the summation in the denominator of eq. (13.12) is taken over all N components of the mixture. Similarly, the segment volume fraction of the solvent, q_1' , is calculated from the weight fractions and the group volume parameter of each component of the mixture, r_j' , as

$$\phi_1' = \frac{r_1' w_1}{\sum_{j=1}^N r_j' w_j} \quad (13.13)$$

where the relative van der Waals volume is given as

$$r_1' = \frac{1}{M_1} \sum_{k=1}^N v_k^{(1)} R_k \quad (13.14)$$

and $v_k^{(1)}$ is the number of groups (an integer) of type k in the solvent and R_k is the normalized van der Waals group volume, V_{wk} , evaluated as

$$R_k = \frac{V_{wk}}{15.17}. \quad (13.15)$$

The molar group area parameter, Q_k , given by eq. (13.11), and the molar group volume parameter, R_k , are available for most structural groups as well as for some common solvents, such as water, carbon disulfide, and dimethylformamide. These group parameters are continuously updated and new ones added in the literature [21]. Some representative values of Q_k and R_k are given in Table 13-6.

It is noted that the first two terms on the RHS of eq. (13.9) are essentially the combinatorial terms of the Flory–Huggins (F–H) equation (eq. 3.37) with the exception that segment rather than volume fractions are used. The remaining two terms serve to correct for the effect of molecular shape. The difference between the combinatorial activity given by eq. (13.9) and that of the F–H expression is usually

small when segment fractions are used in place of volume fractions in the F–H expression.

Table 13-6 Molar Group Area (Q_k) and Volume (R_k) Parameters^a

Main Group	Subgroup	R_k	Q_k	Sample Group Assignment
CH_2	CH_3	0.9011	0.848	Hexane
	CH_2	0.6744	0.540	<i>n</i> -Butane
	CH	0.4469	0.228	2-Methylpropane
	C	0.2195	0.000	Neopentane
$\text{C}=\text{C}$	$\text{CH}_2=\text{CH}$	1.3454	1.176	Hexene-1
	$\text{CH}=\text{CH}$	1.1167	0.867	Hexene-2
	$\text{CH}_2=\text{C}$	1.1173	0.988	2-Methyl-1-butene
	$\text{CH}=\text{C}$	0.8886	0.676	2-Methyl-2-butene
	C=C	0.6605	0.485	2,3-Dimethylbutene
CH_2CO	CH_3CO	1.6724	1.448	Butanone
	CH_2CO	1.4457	1.180	Pentanone-3
ACh^b	ACh	0.5313	0.400	Naphthalene
	AC	0.3652	0.120	Styrene
ACCH_2	ACCH_3	1.2663	0.968	Toluene
	ACCH_2	1.0396	0.660	Ethylbenzene
	ACCH	0.8121	0.348	Cumene
SiO		1.1044	0.466	Polysiloxane
OH		1.0000	1.200	Propanol-2
CH_3OH		1.4311	1.432	Methanol
H_2O		0.9200	1.400	Water
CHCl_3		2.8700	2.410	Chloroform
$\text{HCON}(\text{CH}_3)_2$		3.0856	2.736	<i>N,N</i> -Dimethylformamide
SiO		1.1044	0.466	Octamethyl cyclotetrasilane

^a Supplementary material to ref. [21]

^b The prefix A indicates that the group is contained in an *aromatic* structure.

The residual contribution to the activity of the solvent in UNIQUAC is given as

$$\ln a_1^R = M_1 q_1' \left[1 - \ln \left(\sum_{i=1}^N \theta_i' \tau_{i1} \right) - \sum_{i=1}^N \left(\theta_i' \tau_{i1} / \sum_{j=1}^N \theta_j' \tau_{ji} \right) \right] \quad (13.16)$$

where the two *adjustable* parameters, τ_{ij} and τ_{ji} , are given as

$$\tau_{ij} = \exp \left[- \left(\frac{u_{ij} - u_{jj}}{RT} \right) \right] \quad (13.17)$$

and

$$\tau_{ji} = \exp\left[-\left(\frac{u_{ji} - u_{ii}}{RT}\right)\right]. \quad (13.18)$$

The parameter u_{ij} is the potential energy of aN $i-j$ pair.

In UNIFAC, the *residual* term is replaced by the SOG concept as

$$\ln a_1^R = \sum_{\text{all groups}} v_k^{(1)} \left[\ln \Gamma_k - \ln \Gamma_k^{(1)} \right] \quad (13.19)$$

where Γ_k is the group residual activity (or activity coefficient) and $\Gamma_k^{(1)}$ is the group residual activity (or activity coefficient) of group k in a reference solution containing only solvent molecules (for normalization so that $a_1 \rightarrow 1$ as $w_1 \rightarrow 1$). The group activation term, Γ_k or $\Gamma_k^{(1)}$, is obtained from the expression

$$\ln \Gamma_k = M_k Q'_k \left[1 - \ln \left(\sum_{\text{all groups}} \Theta_m' \Psi_{mk} \right) - \sum_{\text{all groups}} \frac{\Theta_m' \Psi_{km}}{\sum_{\text{all groups}} \Theta_n' \Psi_{nm}} \right] \quad (13.20)$$

where Θ'_m is the *area fraction* of group m , calculated in a similar way to that of θ_j' :

$$\Theta'_m = \frac{Q'_m W_m}{\sum_{n=1}^N Q'_n W_n}. \quad (13.21)$$

In eqs. (13.20) and (13.21), M_k is the molecular weight of the functional group k , Q'_m is the group-area parameter per gram such that $Q'_m = Q_m / M_m$, and W_m is the weight fraction of group m in the mixture. The *group-interaction parameter*, Ψ_{mn} , is given by

$$\Psi_{mn} = \exp\left[-\left(\frac{U_{mn} - U_{nn}}{RT}\right)\right] = \exp\left(\frac{a_{mn}}{T}\right) \quad (13.22)$$

where U_{mn} is a measure of the energy of interaction between groups m and n . The group-interaction parameters, a_{mn} and a_{nm} ($a_{mn} \neq a_{nm}$), for each pair of groups have been compiled and continuously revised, principally by fitting experimental VLE or LLE data for low-molecular-weight compounds. Representative values of the group-interaction parameters derived from VLE data are given in Table 13-7. In tables of group-interaction parameters, each major group contains several subgroups with their own R_k and Q_k values (Table 13-6), but *all subgroups have identical group-interaction parameters*.

Table 13-7 Representative Values of the Group-Interaction Parameters, a_{nm} and a_{mn} (K)^a

	CH₂	C=C	ACH	ACCH₂	OH	CH₂CO	CH₃OH	SiO
CH ₂	0.0	86.02	61.13	76.50	986.5	476.4	697.2	252.7
C=C	-35.36	0.0	38.81	74.15	524.1	182.6	787.6	n.a.
ACH	-11.12	3.446	0.0	167.0	636.1	25.77	637.4	238.9
ACCH ₂	-69.70	-113.6	-146.8	0.0	803.2	-52.10	603.3	n.a.
OH	156.4	457.0	89.60	25.82	0.0	84.00	-137.1	n.a.
CH ₂ CO	26.76	42.92	140.1	365.8	164.5	0.0	108.7	n.a.
CH ₃ OH	16.51	-12.52	-50.00	-44.50	249.1	23.39	0.0	n.a.
SiO	110.2	n.a.	234.4	n.a.	n.a.	n.a.	n.a.	n.a.

^a Supplementary material to ref. [21].

For polymer–solvent systems, Oishi and Prausnitz [17] have shown that the *free-volume* contribution appearing in eq. (13.8) can be a significant *positive* contribution to the total activity and used the Flory EOS (where $X_{12} = 0$) to obtain

$$\ln a_1^{\text{FV}} = 3c_1 \ln \left[\frac{\left(\tilde{v}_1^{1/3} - 1 \right)}{\left(\tilde{v}_M^{1/3} - 1 \right)} \right] - c_1 \left[\left(\frac{\tilde{v}_1}{\tilde{v}_M} - 1 \right) \left(1 - \frac{1}{\tilde{v}_1^{1/3}} \right)^{-1} \right]. \quad (13.23)$$

In this equation, $3c_1$ represents the number of external degrees of freedom per solvent (i.e., component 1) molecule (c_1 is usually set to 1.1), subscript M refers to the mixture, and \tilde{v} is the reduced volume as defined in Chapter 3 (eq. (3.47)). Oishi and Prausnitz have suggested calculating the reduced volume for the solvent as

$$\tilde{v} = \frac{v_1}{15.17br'_1} \quad (13.24)$$

where b is a proportionality factor of order unity (often taken as 1.28). The reduced volume of the mixture, \tilde{v}_M , is calculated by assuming that the volume of the liquid mixture is additive. For a binary mixture of solvent and polymer (component 2), \tilde{v}_M is given as

$$\tilde{v}_M = \frac{v_1 w_1 + v_2 w_2}{15.17b(r'_1 w_1 + r'_2 w_2)}. \quad (13.25)$$

UNIFAC-FV has been very successful in the prediction of solvent activities for polymer solutions [16], as illustrated for polyisobutylene/benzene in Figure 13-3. Although the UNIFAC-FV approach was developed to improve predictions of activities or activity coefficients for polymeric systems, it also has been used for mixtures of low-molecular-weight compounds with reasonable success. Free-volume contributions can be important even for mixtures of low-molecular-weight

components if the characteristic temperatures (T^*) differ significantly, as in the case of gas/hydrocarbon mixtures, for example. As an illustration of UNIFAC-FV, the calculation of the activity of benzene in polyisobutylene is shown in Example 13.6

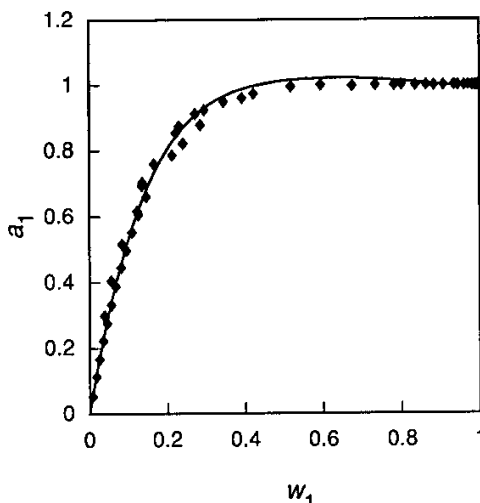
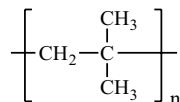


Figure 13-3 Comparison of experimental data for the activity of benzene (a_1) as a function of its weight fraction (w_1) in polyisobutylene at 25°C with predictions (—) of UNIFAC-FV [16].

Example 13.6

Using UNIFAC-FV, calculate the activity of benzene in polyisobutylene (PIB)



at 25°C when the weight fraction of benzene is 0.1.

Solution

Compo- nent	ρ (g mL^{-3})	M	Main group	Sub- group	R_k	Q_k	No. of Groups
Benzene	0.8736	78.11	ACH	ACH	0.5313	0.400	6
PIB	0.9169	56.07	CH ₂	C	0.2195	0.0	1
			CH ₂	CH ₂	0.6744	0.540	1
			CH ₂	CH ₃	0.9011	0.848	2

Combinatorial contribution:

$$q'_1 = \frac{1}{78.11} 6(0.400) = 0.03073$$

$$r'_1 = \frac{1}{78.11} 6(0.5313) = 0.04081$$

$$q'_2 = \frac{1}{56.07} [1(0) + 1(0.540) + 2(0.848)] = 0.03987$$

$$r'_2 = \frac{1}{56.07} [1(0.2195) + 1(0.6744) + 2(0.9011)] = 0.04808$$

$$\theta'_1 = \frac{0.03073(0.1)}{0.0307(0.1) + 0.03987(0.9)} = 0.07888$$

$$\phi'_1 = \frac{0.04081(0.1)}{0.04081(0.1) + 0.04808(0.9)} = 0.08618$$

$$\ln a_i^c = \ln(0.08618) + (1 - 0.08618) + \frac{10}{2}(78.11)(0.03073) \left[\ln\left(\frac{0.07888}{0.08618}\right) - 1 + \frac{0.08618}{0.07888} \right]$$

$$= -1.4831$$

Residual contribution:

$$W_{\text{ACH}} = 0.1$$

$$W_{\text{CH}_3} = 0.9 \frac{15.025(2)}{56.07} = 0.4823$$

$$W_{\text{CH}_2} = 0.9 \frac{14.0169}{56.07} = 0.2250$$

$$W_c = 0.9 \frac{12.001}{56.07} = 0.1926$$

$$Q'_{\text{ACH}} = \frac{Q_{\text{ACH}}}{13.0089} = \frac{0.4}{13.0089} = 0.03075$$

$$Q'_{\text{CH}_3} = \frac{Q_{\text{CH}_3}}{15.025} = \frac{0.848}{15.025} = 0.05644$$

$$Q'_{\text{CH}_2} = \frac{Q_{\text{CH}_2}}{14.0169} = \frac{0.540}{14.0169} = 0.03853$$

$$Q'_c = \frac{Q_c}{12.001} = \frac{0}{12.001} = 0$$

$$\Theta'_{\text{ACH}} = \frac{Q'_{\text{ACH}} W_{\text{ACH}}}{Q'_{\text{ACH}} W_{\text{ACH}} + Q'_{\text{CH}_3} W_{\text{CH}_3} + Q'_{\text{CH}_2} W_{\text{CH}_2} + Q'_c W_c} = \frac{0.003075}{0.03897} = 0.07892$$

$$\Theta'_{\text{CH}_3} = \frac{Q'_{\text{CH}_3} W_{\text{CH}_3}}{Q'_{\text{ACH}} W_{\text{ACH}} + Q'_{\text{CH}_3} W_{\text{CH}_3} + Q'_{\text{CH}_2} W_{\text{CH}_2} + Q'_c W_c} = \frac{0.02722}{0.03897} = 0.6986$$

$$\Theta'_{\text{CH}_2} = \frac{\mathcal{Q}'_{\text{CH}_2} W_{\text{CH}_2}}{\mathcal{Q}'_{\text{ACH}} W_{\text{ACH}} + \mathcal{Q}'_{\text{CH}_3} W_{\text{CH}_3} + \mathcal{Q}'_{\text{CH}_2} W_{\text{CH}_2} + \mathcal{Q}'_{\text{C}} W_{\text{C}}} = \frac{0.008669}{0.03897} = 0.2225$$

$$\Theta'_{\text{C}} = \frac{\mathcal{Q}'_{\text{C}} W_{\text{C}}}{\mathcal{Q}'_{\text{ACH}} W_{\text{ACH}} + \mathcal{Q}'_{\text{CH}_3} W_{\text{CH}_3} + \mathcal{Q}'_{\text{CH}_2} W_{\text{CH}_2} + \mathcal{Q}'_{\text{C}} W_{\text{C}}} = 0$$

Note that interaction parameters are only between main groups, and in this case there are only two main groups—ACH (benzene) and CH₂ (C, CH₂, and CH₃ subgroups)—in PIB. This greatly reduces the number of calculations for the residual contribution to the activity of benzene as follows:

$$\Psi_{\text{ACH},\text{CH}_2} = \exp\left(-\frac{a_{\text{ACH},\text{CH}_2}}{T}\right) = \exp\left(\frac{11.12}{298}\right) = 1.0380 = \Psi_{\text{ACH},\text{CH}_3} = \Psi_{\text{ACH},\text{C}}$$

$$\Psi_{\text{CH}_2,\text{ACH}} = \exp\left(-\frac{a_{\text{CH}_2,\text{ACH}}}{T}\right) = \exp\left(-\frac{61.13}{298}\right) = 0.8145 = \Psi_{\text{CH}_3,\text{ACH}} = \Psi_{\text{C},\text{ACH}}$$

$$\ln \Gamma_{\text{ACH}} = M_{\text{ACH}} \mathcal{Q}'_{\text{ACH}} \left[1 - \ln \left(\Theta'_{\text{ACH}} \Psi_{\text{ACH},\text{ACH}} + \Theta'_{\text{CH}_3} \Psi_{\text{CH}_3,\text{ACH}} + \Theta'_{\text{CH}_2} \Psi_{\text{CH}_2,\text{ACH}} + \Theta'_{\text{C}} \Psi_{\text{C},\text{ACH}} \right) - \frac{\Theta'_{\text{ACH}} \Psi_{\text{ACH},\text{ACH}}}{\Theta'_{\text{ACH}} \Psi_{\text{ACH},\text{ACH}} + \Theta'_{\text{CH}_3} \Psi_{\text{CH}_3,\text{ACH}} + \Theta'_{\text{CH}_2} \Psi_{\text{CH}_2,\text{ACH}} + \Theta'_{\text{C}} \Psi_{\text{C},\text{ACH}}} - \frac{\Theta'_{\text{CH}_3} \Psi_{\text{ACH},\text{CH}_3}}{\Theta'_{\text{ACH}} \Psi_{\text{ACH},\text{CH}_3} + \Theta'_{\text{CH}_3} \Psi_{\text{CH}_3,\text{CH}_3} + \Theta'_{\text{CH}_2} \Psi_{\text{CH}_2,\text{CH}_3} + \Theta'_{\text{C}} \Psi_{\text{C},\text{CH}_3}} - \frac{\Theta'_{\text{CH}_2} \Psi_{\text{ACH},\text{CH}_2}}{\Theta'_{\text{ACH}} \Psi_{\text{ACH},\text{CH}_2} + \Theta'_{\text{CH}_3} \Psi_{\text{CH}_3,\text{CH}_2} + \Theta'_{\text{CH}_2} \Psi_{\text{CH}_2,\text{CH}_2} + \Theta'_{\text{C}} \Psi_{\text{C},\text{CH}_2}} - \frac{\Theta'_{\text{C}} \Psi_{\text{ACH},\text{C}}}{\Theta'_{\text{ACH}} \Psi_{\text{ACH},\text{C}} + \Theta'_{\text{CH}_3} \Psi_{\text{CH}_3,\text{C}} + \Theta'_{\text{CH}_2} \Psi_{\text{CH}_2,\text{C}} + \Theta'_{\text{C}} \Psi_{\text{C},\text{C}}} \right] =$$

$$0.400 [1 - \ln(0 + 0.2225 \cdot 0.8145 + 0.6986 \cdot 0.8145 + 0.07892) - \frac{0.07892(1)}{0.07892(1) + 0.6986(0.8145) + 0.2225(0.8145) + 0} - \frac{(0.6986 + 0.2225)(1.0380)}{0.0789(1.0380) + 0.6986(1) + 0.2225 + 0}] = 0.4 [1 - \ln(0.8292) - 1.0615] = 0.05036$$

$$\ln \Gamma_{\text{ACH}}^{(1)} = 0$$

$$\ln a_i^R = 6(0.05036 - 0) = 0.3022$$

Free-volume contribution:

$$\tilde{\nu}_1 = \frac{1.145}{15.17(1.28)0.04081} = 1.445$$

$$\tilde{\nu}_M = \frac{1.1447(0.1) + 1.0906(0.9)}{15.17(1.28)[0.04081(0.1) + 0.04808(0.9)]} = 1.1920$$

$$\ln a_1^{\text{FV}} = 3(1.1) \ln \left[\frac{1.445^{1/3} - 1}{1.1920^{1/3} - 1} \right] - 1.1 \left[\left(\frac{1.445}{1.1920} - 1 \right) \left(1 - \frac{1}{1.445^{1/3}} \right)^{-1} \right] = 0.528$$

Total activity of benzene:

$$\ln a_1 = -1.483 + 0.302 + 0.528 = -0.653; a_1 = 0.520$$

These results show that the residual or enthalpic contribution to the activity is relatively small compared to the combinatorial contribution. This should be expected on the basis of the non-polar nature of PIB and benzene. As shown by a comparison of experimental activities with calculated values in Figure 13-3, UNIFAC-FV very accurately predicts the activity of benzene in PIB due to the extensive parameterization of UNIFAC for many compounds.

13.2 Topological Indices

Another method of predicting polymer properties is the topological approach developed by Bicerano [4, 22]. This approach uses simple connectivity indexes and other structural descriptors where the emphasis is on the use of additive contributions over individual atoms and bonds rather than chemical groups. This method is limited to amorphous, uncrosslinked, isotropic polymers containing any of nine atoms (i.e., C, N, O, H, F, Si, S, Cl, and Br). All that is required is the structure of the repeat unit and its molecular weight. Details of the procedures required are given in Bicerano's book [4] and have been incorporated in the commercial software program Synthia.* Properties that can be calculated include the van der Waals volume (V_w), molar volume, solubility parameter, glass-transition temperature, coefficient of volumetric thermal expansion, molar volume as a function of temperature, molar heat capacity at constant pressure, permeability (O_2 , N_2 , CO_2), molar diamagnetic susceptibility, molar refraction, dielectric constant, thermal conductivity, viscosity, activation energy for viscous flow, characteristic ratio, critical molecular weight for entanglement, mechanical properties (Young's modulus, volume resistivity, brittle fracture stress, bulk modulus, shear yield stress, shear modulus), refractive index, and surface tension. Hand calculations are tedious as illustrated by the example of polystyrene given in Bicerano's reference article [22] but lend themselves nicely to computer implementation.

In general, the most basic information required is the structure of the repeat unit of the polymer chain from which the molecular weight of the repeat unit can be calculated. For polystyrene (PS) whose repeat unit structure is shown in Figure

* Available through Materials Studio (Accelrys).

13-4, the molecular weight per repeat unit is 104.15 g/mol. The first step is the calculation of the total number of rotational degrees of freedom of the polymer repeat unit. The total number is obtained from the sum of the total number of backbone degrees of freedom and the total number of side-group degrees of freedom using a set of specific rules to define a rotational unit. In the case of PS, there is a total of two rotatable backbone bonds in the backbone and just one rotational side-group bond (i.e., the bond connecting the phenyl ring and the backbone) for a total of three rotational degrees of freedom as shown in Figure 13-4. The next step is the calculation of the length of the polymeric repeat unit in its fully extended conformation (i.e., the planar zig-zag conformation in the case of PS) as shown in Figure 13-4. This is obtained by calculating the length of a triangle with two sides formed by the C–C bonds 1 and 2 (1.54 Å in length) connected by an angle of 109.5°. For PS, this value is 2.54 Å.

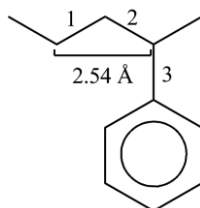


Figure 13-4 Representation of the repeat unit structure of polystyrene showing the two rotatable backbone bonds (1 and 2) and the rotatable side-group bond (3). For clarity, carbon and hydrogen atoms have been omitted. The length of the repeat unit, based upon the planar zig-zag conformation of the backbone chain, is 2.54 Å.

The next step is the calculation of the connectivity indices. These include the two zeroth-order indices, ${}^0\chi$ and ${}^0\chi^v$, defined in terms of *atom* descriptors and two first-order indices, ${}^1\chi$ and ${}^1\chi^v$, defined in terms of *bond* descriptors. The zeroth-order indices are calculated from the atomic indices, δ , and valence atomic indices, δ^v , as

$${}^0\chi \equiv \sum \left(1/\sqrt{\delta} \right) \quad (13.26)$$

and

$${}^0\chi^v \equiv \sum \left(1/\sqrt{\delta^v} \right) \quad (13.27)$$

where the summation is made over all the vertices of the hydrogen-suppressed repeat unit. Bond indices are calculated from the atomic indices as

$$\beta_{ij} \equiv \delta_i \delta_j \quad (13.28)$$

and

$$\beta_{ij}^v = \delta_i^v \delta_j^v. \quad (13.29)$$

The first-order (bond) connectivity indices are obtained from the bond indices as

$${}^1\chi \equiv \sum \left(1/\sqrt{\beta} \right) \quad (13.30)$$

and

$${}^1\chi^v \equiv \sum \left(1/\sqrt{\beta^v} \right). \quad (13.31)$$

The atomic indices, δ , and valence atomic indices, δ' , are obtained from tables of values that depend upon the type and hybridization (Hyb) of atoms at the vertices and the total number of hydrogen atoms (N_H) at these sites. Some representative values are given in Table 13-8. Application of these rules to the example of PS is shown by values marked on a repeat unit in Figure 13-5. Using these values gives values of the zeroth-order indices, ${}^0\chi$ and ${}^0\chi^v$, and the first-order indices, ${}^1\chi$ and ${}^1\chi^v$ from eq. (13.26) through eq. (13.31). The calculated values are ${}^0\chi = 5.40$, ${}^0\chi^v = 4.67$, ${}^1\chi = 3.97$, and ${}^1\chi^v = 3.02$. Once these values are available, various physical, thermal, and mechanical properties can be calculated from the appropriate equation given by Bicerano [4]. As an example, density can be obtained from the repeat molecular weight, M , and the amorphous molar volume at 298 K, $V(298)$, as

$$\rho = \frac{M}{V(298)} \quad (13.32)$$

where

$$V(298) = 3.642770 {}^0\chi + 9.798697 {}^0\chi^v - 8.542819 {}^1\chi + 21.693912 {}^1\chi^v + 0.978655 N_{MV} \quad (13.33)$$

and N_{MV} is calculated from the overall chemical composition of the repeat unit. Predicted physical and thermal properties of PS calculated by Bicerano's method are compared with experimental values in Table 13-9. In general, agreement is very good.

**Table 13-8 Selective Atomic and Valence
Atomic Indices [22]**

Atom	Hyb	N _H	δ	δ ^v
C	sp ³	3	1	1
		2	2	2
		1	3	3
		0	4	4
	sp ²	2	1	2
		1	2	3
		0	3	4
	sp	1	1	3
		0	2	4
	N	sp ³	2	1
		1	2	4
		0	3	5
O	sp ²	1	1	4
		0	2	5
	sp	0	1	5
	sp ³	1	1	5
Si	sp ³	0	2	6
		0	1	6
	sp ³	1	3	1/3
Cl	—	0	4	4/9
		0	1	7/9

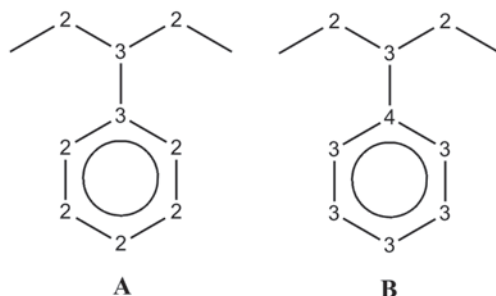


Figure 13-5 Atomic (**A**) and valence atomic (**B**) connectivity indices marked at the vertices of a PS repeat unit. Values taken from Table 13-8.

Table 13-9 Comparison Between Experimental Physical and Thermal Properties and Properties Estimated by Bicerano's Method [22]

Property	Predicted Value	Experimental Value
ρ , g cm ⁻³	1.07	1.05
δ_s , (J cm ⁻³) ^{0.5}	19.5, 20.1	17.4- 19.0
T_g , K	382	373
C_p^g , (298), J/(mole K)	133.5	126.5
$\Delta C_p(T_g)$	26.8	30.8
γ , dyn cm ⁻¹ at 298 K	39.4, 41.0, 43.6	40.7

13.3 Artificial Neural Network

An artificial neural network (ANN) is a computing system composed of a number of highly connected processing elements or nodes that process input data and predict specific output data in a way roughly similar to the function of brain neurons. Each neural network has a learning process that typically includes a set of training data for which the output is known. A schematic representation of a simple ANN is illustrated in Figure 13-6. This neural network has five input nodes (X_1 , X_2 , X_3 , X_4 , and X_5), one output node (Y_1), and four hidden nodes represented by the shaded circles. During operation of the ANN, each of the input variables is assigned a weight, W_i . As shown, each input node is able to provide signals to the other nodes. The weighted sum of all the signals is then transformed by a specific function. The output variable can be changed by adjusting the weights to each node.

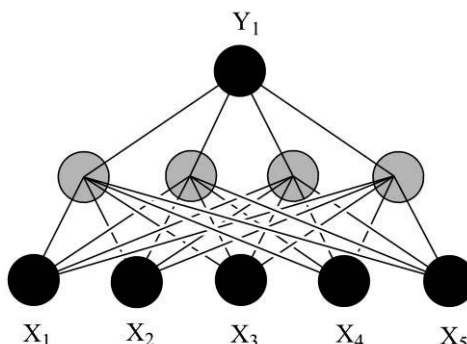


Figure 13-6 Illustration of a simple neural network consisting of five input nodes (X_1 through X_5), four hidden nodes (shaded circles), and a single output node (Y_1).

Each node beyond the input layer takes as its input a linear combination of the outputs. For example, the input to some i th node in the hidden layer, I_i , can be written as

$$I_i = \sum_j w_{ij} X_j + \theta_i \quad (13.34)$$

where X_j is the output of the j th node, θ_i is a parameter termed the *bias*, w_{ij} is the connection weight between the nodes, and the summation is over all the nodes in the previous layer. Weights can have positive or negative values. The calculated input is then transformed to calculate the output of the nodes. A common transform function is an S-shaped sigmoid function such as

$$y(x) = -\frac{a}{c[1 - \exp(-bx)]}. \quad (13.35)$$

Radial and threshold transfer functions also have been used. Weights are iteratively changed in proportion to the differences between the obtained outputs and target values in the training set. A set of input and known output values constitutes a training set for the network whereby the connection weights and biases are adjusted to minimize the prediction error. While several neural-network configurations are possible, a commonly used approach is the back-propagation neural network (BPNN). There are at least three hierarchical layers of neural nodes in a BPNN—an input layer, a middle or hidden layer, and an output layer as illustrated in Figure 13-6. In this configuration, each layer is fully connected to the next layer. The number of nodes in the hidden layer can be adjusted depending upon the complexity of the problem and the size of the input information.

Traditional applications of ANNs include speech recognition and synthesis, pattern recognition, market forecasting, process modeling, and property prediction. The last two have significant applications in polymer science and technology and include the design of compression molding, blow molding, and injection molding and such diverse property predictions as density, permeability, solvent activity, the compressibility factor, phase equilibria, permeability, dielectric dissipation factor, lower critical solution temperatures, estimation of kinetic rate constants in metallocene polymerization, and failure prediction of composites. ANNs have also been combined with topological indices to predict polymer properties [23]. An example [24] of the application of ANNs to predict polymer T_g is discussed next.

Prediction of T_g . As discussed earlier, group-contribution methods can be used with good success but only if the specific chemical groups of the target polymer are available in the correlation. There have been a number of approaches using different polymer descriptors, typically obtained from computational chemistry cal-

culations. One recent example [24] is the prediction of T_g using molecular descriptors obtained from density functional theory (DFT) calculations. Descriptors include total energy, C_v , molecular average polarizability, the energy of the highest occupied molecular orbital, and entropy. Experimental T_g values for a total of 113 polyacrylates and polystyrenes were used for this study. From these, 58 polyacrylates were selected for training a three-layer BPNN. The 23 polyacrylates and 32 polystyrenes were used to evaluate the performance of the neural network. In Figure 13-7, results are presented in a plot of calculated versus experimental T_g values. As illustrated, agreement is good. Specifically, the root-mean-square error for the prediction set was 17 K.

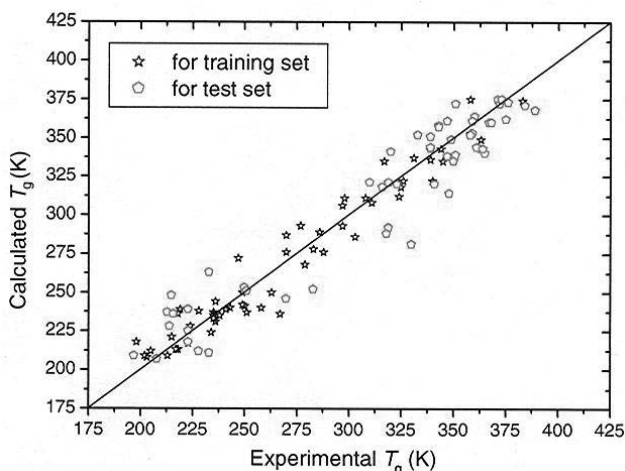


Figure 13-7 Plot of calculated versus experimental T_g obtained by using an ANN of chemical descriptors. Reproduced from W. Liu and C. Cao, *Artificial Neural Network Prediction of the Glass Transition Temperature of Polymers*. Colloid and Polymer Science, 2009. **287**: p. 811–818. Copyright 2009 Springer-Verlag.

A comparison of different methods for prediction of T_g of a polyacrylate and a polystyrene common to published group-contribution [2], graft theory [4], and ANN [24] methods is given in Table 13-10. As shown, no method is uniformly successful as is illustrated in the case of the poly(nonyl acrylate), where the best prediction is graph theory, and in the case of poly(4-*sec*-butylstyrene), where the ANN gives the best result. ANN has the advantage that prior parameterization is not necessary; however, obtaining computational data for repeat units is a time-consuming process. The T_g can also be obtained from molecular dynamics simulations as discussed in Section 13.4.3; however, this too is very time-consuming and requires a robust mo-

lecular force field that has been parameterized for the functional groups present in the polymer under study.

Table 13-10 Comparison of Experimental T_g with Values Predicted by ANN, Graph Theory, and Group-Contribution Methods

Polymer	Exp. T_g (K)	ANN [24]	Graph Theory [4]	Group Contribution [2]
Poly(nonyl acrylate)	215	248	220	204
Poly(4- <i>sec</i> -butylstyrene)	359	361	352	344

13.4 Molecular Simulations

Computational (quantum) chemistry provides approximate solutions to the Schrödinger wave equation from which molecular geometries and energies can be obtained. These are called *ab initio* methods. A related approach is density functional theory (DFT). Both approaches require significant computer time and are useful only in the study of small molecules and molecular clusters. In the case of large molecules such as biomolecules or polymers, molecular dynamics (MD) can be used to determine physical, mechanical, and transport properties, including density, self-diffusion coefficients, modulus, phase-equilibrium behavior, X-ray and neutron diffraction spectra, and glass-transition temperatures. Another approach is the use of stochastic methods* such as Monte Carlo (MC) simulations that provide a probabilistic description of events. Monte Carlo techniques represent a statistical sampling process that can be applied to a system with a large number of particles or to explore molecular structure over long time scales or to sample a large region of computational space. MC calculations can be used to determine phase equilibrium and sorption isotherms. Using robust molecular force fields parameterized for polymers as described in the following section, polymer properties can be obtained with considerable accuracy and reliability using MD or MC simulations.

Early MD applications used both atomistic and united-atom (UA) simulations. As illustrated in Figure 13-8, each atom is treated individually in the parameterization and dynamics calculation in atomistic simulations. In UA simulations (Figure 13-8), hydrogen atoms are united with a “heavy” atom such as carbon to form a single species that is separately parameterized. Combined with a simple force field as described in Section 13.4.1, the use of a UA representation reduces the simulation

* A stochastic variable is one that does not depend in a completely definite way upon the independent variable but is subject to random effects that can only be defined in statistical terms.

(CPU) time with some loss in the quality of the results. UA representations have been used in the simulation of large biological systems such as proteins. A related approach that is becoming an important tool in the simulation of both biological and polymeric systems is the use of *coarse-grained* (CG) [25, 26] representation of molecular systems where a chemical grouping such as a methylene linkage or an aromatic ring is represented by one or more CG “beads” as illustrated in Figure 13-9. Force field parameterization for CG systems is much more challenging and more specific to a particular protein or polymer than in atomistic or UA simulations but can greatly accelerate dynamics time and, therefore, extend the temporal and spatial range that can be studied. Specific applications where CG simulations can be useful include simulations of self-assembly of surfactants and block copolymers. CG simulations are beyond the scope of the introductory treatment of molecular simulations given in this chapter and, therefore, the reader is encouraged to consult the excellent journal articles and books [27] in this area. A brief discussion of important CG force fields is given at the end of Section 13.4.1.

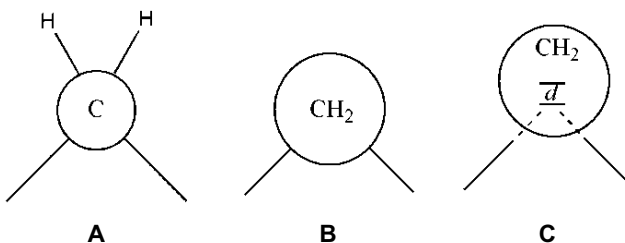


Figure 13-8 Comparison of different atomic representations of a methylene repeat unit. **(A)** Atomistic atom; **(B)** united atom (UA); and **(C)** anisotropic united atom (AUA). In the case of AUA, the parameter d represents the offset of the effective non-bonded center from the atomic center of the carbon atom. UA representation with this adjustable offset was used to improve the quality of UA simulations.

Monte Carlo Simulations. The use of Monte Carlo methods received significant impetus with the development of digital computers in the late 1940s. The most important application of Monte Carlo techniques utilizes statistical sampling procedures, principally the Metropolis or the Monte Carlo Markov chain (MCMC) method [28]. Important applications for Monte Carlo methods in polymer science include the simulation of phase equilibrium and also sorption isotherms as illustrated in Section 13.5.8.

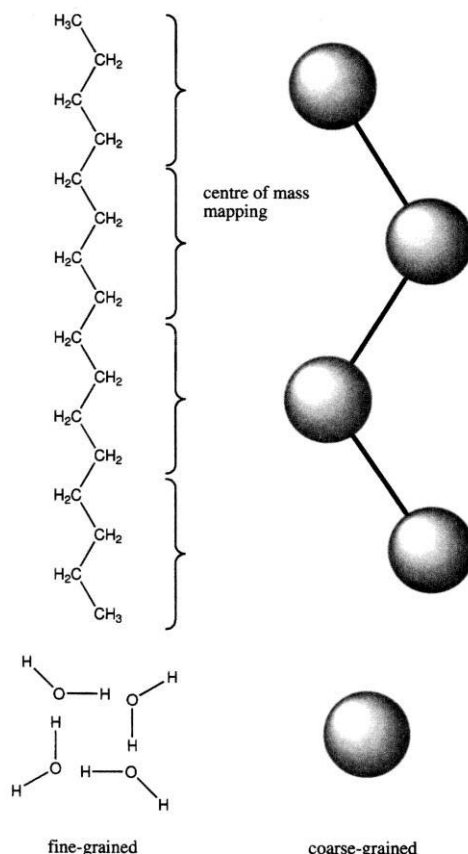


Figure 13-9 Comparison between atomistic (left-hand side) and CG representations of polyethylene and water (right-hand side). In the case of PE, three methylene groups are replaced by a single CG bead while a cluster of three water molecules is represented by one CG bead. Reproduced from M. Christen, and W. F. van Gunsteren, *Multigraining: An Algorithm for Simultaneous Fine-Grained and Coarse-Grained Simulation of Molecular Systems*. Journal of Chemical Physics, 2006, **124**(15): p. 154106.

13.4.1 Molecular Mechanics Force Fields

The success of such MD and MC methods depends upon the quality of a force field that describes the potential energy, U , of the molecular system as the sum of all bonded (U^B) and non-bonded (U^{NB}) terms as

$$U(\mathbf{r}) = U^B(\mathbf{r}) + U^{NB}(\mathbf{r}). \quad (13.36)$$

The bonded terms include potential energy contributions from bond-stretching, angle-bending, and dihedral (or torsional) contributions as

$$V^B(r) = \sum_{\text{bonds}} V^{\text{bond}}(r_{ij}) + \sum_{\text{bends}} V^{\text{bend}}(\theta_{ijk}) + \sum_{\text{dihedral}} V^{\text{tors}}(\phi_{ijkl}) \quad (13.37)$$

where r_{ij} is the distance between two consecutive bonded atoms i and j , θ_{ijk} is the valence angle between three consecutive atoms i, j, k , and ϕ_{ijkl} is the torsional (dihedral) angle between four consecutive atoms i, j, k, l . Each summation is made over all contiguous atoms constituting bonds (i.e., two-body interactions), angles (i.e., three-body interactions), and torsions (i.e., four-body interactions) in the system. Non-bonded terms typically include steric (i.e., Lennard-Jones or LJ) and electrostatic (i.e., Coulombic) terms. Schematic representations of the bonded (i.e., bond-stretching, angle-bending, and torsion or dihedral) and non-bonded (i.e., LJ and Coulombic) contributions to the potential energy of a molecular systems are shown in Figure 13-10.

Force field parameters for each bonded or non-bonded term are obtained by fitting potential energy terms to potentials of small molecules calculated by *ab initio* or DFT methods or by fitting to experimental data such as crystal structure and the heat of vaporization (ΔH_v) for low-molecular-weight compounds. Examples of *bonded* contributions include simple harmonic functions for bond stretching

$$U^{\text{bond}}(r_{ij}) = \frac{1}{2} \sum_{\text{bonds}} k_{ij}^{\text{bond}} (r_{ij} - r_{ij}^{\circ})^2 \quad (13.38)$$

where k_{ij}^{bond} is the bond-stretching parameter and r_{ij}° is the equilibrium bond distance (for which the potential energy contribution is zero). Among alternative forms for the bond-stretching term is the *quartic* expression used in modern force fields

$$U^{\text{bond}}(r_{ij}) = \frac{1}{2} \sum_{\text{bonds}} \left[k_2 (r_{ij} - r_{ij}^{\circ})^2 + k_3 (r_{ij} - r_{ij}^{\circ})^3 + k_4 (r_{ij} - r_{ij}^{\circ})^4 \right] \quad (13.39)$$

where k_2 , k_3 , and k_4 are parameters for individual $i-j$ atom pairs forming covalent bonds. Similar harmonic and quartic terms have been used for angle bending. Torsional contributions to the bonded potential include the form

$$U^{\text{tors}}(\phi_{ijkl}) = \frac{1}{2} \sum_{\text{dihedrals}} \sum_{n=1,2,\dots} k_{ijkl}^{\text{tors}}(n) [1 - \cos(n\phi_{ijkl})] \quad (13.40)$$

where n is the periodicity of the torsional motion and the summation is over all torsional angles for each periodicity. Other forms of torsional terms are available including terms for out-of-plane bending for co-planar structures as illustrated in Figure 13-10.

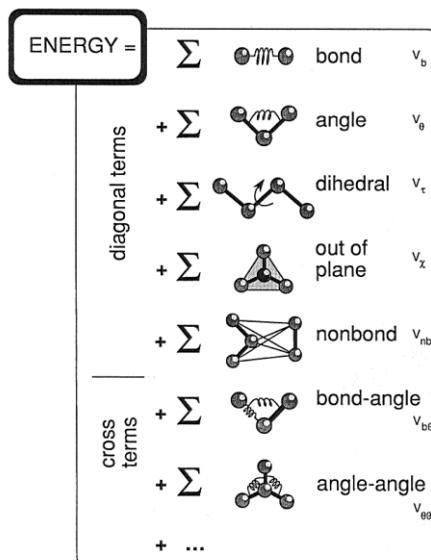


Figure 13-10 Model representation of atoms participating in potential terms found in a typical molecular force field. Diagonal terms refer to interactions that can be expressed as a function of single internal coordinates such as bond stretching or angle bending. Cross-terms represent coupled interactions involving two or more coordinates such as interactions between atoms participating simultaneously in bond stretching and angle bending. Reproduced from U. Dinur and A. T. Hagler, *New Approaches to Empirical Force Field*, in *Reviews in Computational Chemistry*, K. B. Lipkowitz and B. D. Boyd, eds. 1991, New York: VCH Publishers, Inc., p. 99–164. Reprinted by permission of John Wiley & Sons.

Cross-coupling terms are used in many force fields to represent the interrelationship between one type of deformation and another such as between bond stretching and torsional rotation and between bond stretching and angle bending as quantified in eq. (13.41).

$$U^{b,b}(r_{ij}, \theta_{ijk}) = \frac{1}{2} \sum_{\text{bonds}} \sum_{\text{bends}} k^{b,b} (r_{ij} - r_{ij}^o)^2 (\theta_{ijk} - \theta_{ijk}^o)^2 \quad (13.41)$$

Non-bonded terms include intramolecular interactions between pairs of atoms separated by three or more bonds and those belonging to different molecules (i.e., intermolecular interactions). Interactions between pairs of atoms separated by one or two bonds are contained in the bonded energy terms of the bond-stretch and angle-bending terms, respectively. All interactions in a simulation system may be included (i.e., Ewald [31] summation) or distance cutoffs (typically in the range from 8 to 12 Å) may be used. Examples of non-bonded terms include Lennard-Jones (LJ) potential (e.g., LJ 6–12) or the LJ 6–9 potential given as

$$U^{\text{LJ}} = \sum_{i \neq j} \epsilon_{ij} \left[2 \left(\frac{r_{ij}^{\circ}}{r_{ij}} \right)^9 - 3 \left(\frac{r_{ij}^{\circ}}{r_{ij}} \right)^6 \right] \quad (13.42)$$

In this case, the sixth order term represents dispersion (i.e., long-range) interactions and the ninth (or twelve) order term represents short-range repulsion. As illustrated by Figure 13-11, the parameters ϵ_{ij} and r_{ij}° appearing in eq. (13.42) are the depth and the distance at the minimum energy of the LJ potential energy function, respectively.

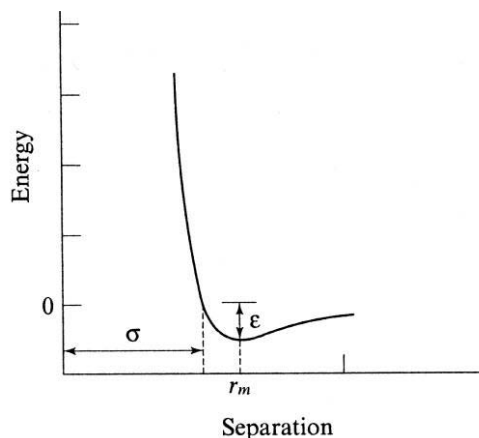


Figure 13-11 The Lennard-Jones potential showing the depth of the potential energy well, ϵ . Reproduced from A. R. Leach, *Molecular Modelling: Principles and Applications*. 2nd ed. 2001, Upper Saddle River: Prentice Hall.

The other non-bonded contribution is the electrostatic potential represented by a Coulombic expression such as

$$U^{\text{es}} = \sum_{i \neq j} \frac{f q_i q_j}{r_{ij}} \quad (13.43)$$

where q_i represents the charge on atom i of the atom pair $i-j$, r_{ij} is the separation between atoms i and j , and $f = 1/\pi\epsilon_0$ where ϵ_0 is the dielectric constant of the medium.

Force fields can be relatively simple with parameterization suitable for a wide number of different molecular structures. While not as robust as more complete force fields, parameterization of these generic force fields can be easily customized for specific polymers. An example is the DREIDING force field [32] that has been used for molecular simulation of a number of different polymers [33]. DREIDING uses a simple harmonic bond-stretching term eq. (13.38) and a harmonic cosine form of the angle-bending term given by eq. (13.44):

$$U^{\text{bend}}(\theta_{ijk}) = \frac{1}{2} \sum_{\text{bends}} k_{ijk}^{\text{bend}} (\cos \theta_{ijk} - \cos \theta_{ijk}^{\circ})^2. \quad (13.44)$$

As reviewed in detail in another publication [33], additional force fields that have been used in the molecular simulations of polymers include GROMOS* [34], CVFF† [35], PCFF,‡ and COMPASS§ [36]. COMPASS is a robust “Class II” force field that is based upon PCFF and makes extensive use of both anharmonic and cross-coupling terms. Parameterization uses results of *ab initio* calculations of small molecules and condensed-phase experimental properties as is the case for its predecessors CVFF and PCFF. The functional form of COMPASS includes quartic expressions for the bond-stretching and angle-bending terms, four cross-coupling terms, and an LJ 9–6 potential. *Parameterization of COMPASS is especially suited for a wide variety of polymer structures* [37].

Reactive Force Fields. Traditional force fields for MD simulations are unable to model chemical reactions due to their inability to accommodate bond breaking and making. In order to extend the capability of traditional molecular mechanics force fields to chemical events, several reactive force fields have been developed. These include the use of partial bond orders to modify the reactive potential energy surface. One of these is MD.REACT, which has been used to model the thermal degradation of polymers [38, 39]. A more recent approach is ReaxFF [40], which has been used to model the thermal decomposition of polydimethylsiloxane [41] as an example.

CG Force Fields. Several force fields have been used for CG simulations. These include the generic MARTINI [42–44] and the Shinoda [45] force field de-

* GROningen MOlecular Simulation.

† Consistent Valence Force Field.

‡ Polymer Consistent Force Field.

§ Condensed-phase Optimized Molecular Potentials for Atomistic Simulation Studies.

veloped to simulate the self-assembly of surfactants, a computationally expensive simulation for fully atomistic simulation. In the case of the MARTINI force field, there is a four-to-one mapping whereby four heavy atoms (excluding hydrogen) are represented by a single interaction center with the exception of ring molecules where there is a two-to-one mapping (e.g., benzene is represented by six beads). In the case of water, four molecules are represented by a single bead. CG force fields can be parameterized and validated from atomistic simulations and experimental data such as pair-correlation functions as discussed in Section 13.5.4. In the case of the MARTINI force field, the *bonded* contribution to the potential energy between connected CG sites includes harmonic bond and dihedral angle terms, which in its simplest form is given as

$$U^B = \frac{1}{2} K_{\text{bond}} (R - R_{\text{bond}})^2 + \frac{1}{2} K_{\text{angle}} [\cos(\theta) - \cos(\theta_0)]^2 \quad (13.45)$$

where K_{bond} and K_{angle} are force constants ($1250 \text{ kJ mol}^{-1} \text{ nm}^{-2}$ and $25 \text{ kJ mol}^{-1} \text{ rad}^{-2}$, respectively), R_{bond} is the equilibrium distance (0.47 nm), and θ_0 is the equilibrium bond angle (180°). The non-bonded contributions include a LJ 6–12 steric potential and a Coulombic electrostatic potential function.

13.4.2 Molecular Dynamics and Monte Carlo Methods

As mentioned earlier, the two principal approaches used in molecular simulations are molecular dynamics (MD) and Monte Carlo (MC) methods. MD methods were used for the first time in the 1970s for molecular simulation of proteins. In MD simulations, an initial position and velocity are assigned for each atom. Forces acting on each atom are then calculated from the potential energy function given by the molecular force field as described in the previous section, and new positions and velocities are calculated at the end of a very small time step, typically a femtosecond (10^{-15} s).

In the case of MD simulations, the time step should be at least one order of magnitude smaller than the shortest periodic motion in the system. For example, the shortest periodic motions are stretching vibrations of hydrogen bonds (e.g., C–H and N–H stretching) that fall in the order of ca. 10^{-14} s^{-1} in frequency. This small time step has significant consequences in terms of the computer time required for the simulation of real molecular processes since calculation of 1000 time steps provides only 1 ps of simulation time and 1 million time steps only 1 ns! If it takes 1 sec to compute one dynamics step, then a 1-ns simulation will take 278 h (ca. 12 days) of CPU time. The relatively “large” time scales of natural events such as fluid flow, phase separation, the diffusion of large molecules, and the conformational

folding of even the smallest proteins can extend to milliseconds, which makes atomistic simulation of such events impractical even on the largest computer platforms. As the simulation system increases in size, a single MD step takes greater CPU time following an N^2 rule where N represents the number of atoms in the simulation system. Simulations of systems containing 100,000 or even 1 million atoms are not uncommon. For simulation of such “large” systems and for long simulation times (e.g., >10 ns), non-atomistic approaches such as coarse-grained and dissipative particle dynamics can be used to shorten computer time; but expansion of the simulation time-size scale is achieved at the expense of molecular detail.

Positions within a Cartesian coordinate system may be determined as a function of time from the molecular mechanics potential-energy function (see Section 13.4.1) simply through Newton’s law of motion written in the form

$$F = \frac{dp}{dt} (= ma) \quad (13.46)$$

where F is force, p is momentum ($p = mv$), m is mass, and a is acceleration. Since F is the negative derivative (i.e., the gradient*) of the potential energy, U , while a is obtained as the second derivative of the atomic positions (x_i) with respect to time, we can write for Cartesian coordinates the following form of eq. (13.46):

$$m\ddot{x}_i = -\nabla U_i. \quad (13.47)$$

Equation (13.47) can be numerically integrated with respect to time to find the trajectory (i.e., x_i) of each atom in the system as a function of time. Forces are computed by calculating an analytical derivative over some small time interval or *time step*. At the end of this interval, a new set of coordinates and velocities is obtained. Algorithms include the standard Verlet derivation [46] and the leapfrog algorithm [47]. Two commonly used algorithms for integrating the equations of motion with internal constraints such as fixing specific bond lengths and angles are called SHAKE [48] and RATTLE [49]. These have the advantage of saving computational time by allowing larger time steps (e.g., 2 fs) when performing MD simulations of systems containing large molecules such as proteins and polymers.

Periodic Boundary Conditions. In the simulation of liquids, solutions, and solids, periodic boundary conditions are used to minimize boundary effects associated

* The gradient of the potential energy is given as

$$\nabla V_i = \frac{\partial V}{\partial x_1} + \frac{\partial V}{\partial x_2} + \frac{\partial V}{\partial x_3}.$$

with small simulation cells (often only 30 to 40 Å along a side). The size of the cell strongly affects the computer time required for a given period of dynamics. In fact, simulation time is directly related to the square of the number of atoms in the system if no cutoff is used. Under periodic conditions, a simulation box, typically a cube or orthorhombus, is virtually surrounded by an infinite number of identical cells as shown in Figure 13-12. Macroscopic systems such as a solution or crystalline solid can be simulated by constructing a unit cell with periodic boundary conditions. Properties that can be obtained from simulation include estimation of transport properties such as the diffusion coefficient. The use of periodic conditions is most appropriate in the case of crystalline systems that have ordered, periodic structures. In the case of amorphous systems such as solutions or liquids, periodicity can be an artifact affecting simulation results if sufficient care is not exercised in the specification of the size of the periodic box.

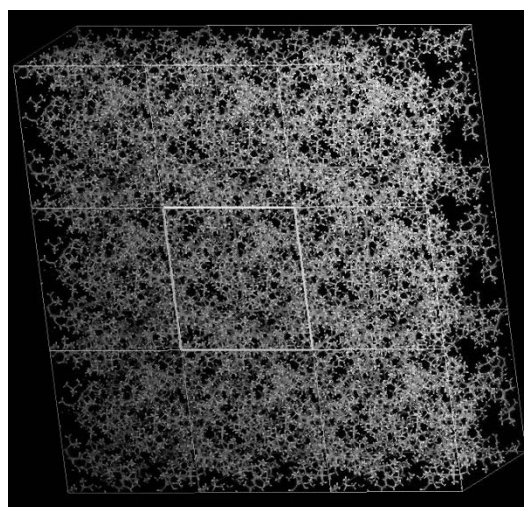


Figure 13-12 Illustration of an amorphous periodic cell containing a polymer chain surrounded by eight identical cells in a periodic structure.

Ensembles. In a molecular simulation, the number of particles and the temperature, pressure, energy, or volume can be held constant. Which variables are held constant and which are allowed to vary define the ensemble. The choice of a particular ensemble is dictated by the property that is the target of the simulation. An example is the *microcanonical* or *NVE* ensemble where N indicates that the number of atoms is held constant as are volume and total energy. In the case of the *canonical* or *NVT* ensemble, energy is exchanged with a heat bath in order to maintain a constant (thermodynamic) temperature at constant volume. This ensemble is useful to sample conformational space because energy can be taken from the heat bath to

overcome rotational barriers as well as to calculate diffusion coefficients. Common thermostats used to control temperature include the Nosé [50], Hoover [51], Andersen [52], and Berendsen [53] methods. A third commonly used ensemble is the isothermal-isobaric or *NPT* ensemble where both pressure and temperature are held constant. Berendsen [53] or Andersen [52] *barostats* are often used for *NPT* dynamics. They are also used to obtain density at a fixed temperature or pressure. A fourth ensemble is the *grand canonical* (μVT) for which chemical potential (μ), volume, and temperature are held constant in the simulation. Grand canonical Monte Carlo (GCMC) simulations are used for the simulation of sorption isotherms in zeolites and polymers as will be discussed in Section 13.5.8.

13.5 Applications of Molecular Simulations

Once a fully equilibrated cell is obtained, typically through a series of NVT and NPT dynamics, the simulation cell can be analyzed to provide a number of important properties. As illustrated in the following sections, these include PVT data such as density and thermal-expansion coefficients, X-ray and neutron-scattering spectra, thermal transition temperatures, permeability, modulus, phase behavior, adsorption isotherms, solubility parameters, and the pair-correlation function (PCF), which can be used to identify polymer interactions such as hydrogen bonding in polyamides. When available, experimental data can be used to validate a particular force field for use with a particular class of polymers.

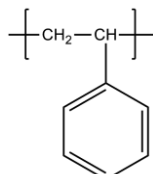
13.5.1 PVT Simulation

PVT data can be obtained from NPT dynamics where the pressure and temperature are held constant and the final volume of a cell is obtained after equilibration. For this purpose, a good thermostat (e.g., Andersen [52]) and barostat (e.g., Berendsen [53]) are required to control temperature and pressure, respectively. Pressure control is the more difficult to control closely, especially when the periodic cells are small. Fortunately, pressure has only a small influence on condensed-phase properties. Results of the analysis of NPT dynamics of an amorphous cell of atactic polystyrene are illustrated in Example 13.7.*

* Example problems shown in this section can be solved by using different force fields and a number of freeware and commercial programs such as Materials Studio (Accelrys, San Diego, CA).

Example 13.7

Using MD solutions, determine the density and solubility parameters of polystyrene (PS) at 298 K.



Solution

For this simulation, the COMPASS force field was selected. Two amorphous cells of PS were constructed. One cell contained a single PS chain having 80 repeat units (RUs) and the other cell contained two PC chains each having 80 RUs. The cell was equilibrated using 25-ps NVT dynamics at 298 K followed by sequential NPT dynamics of 25 ps, 225 ps, and 250 ps, giving a total of 500-ps NPT dynamics. The Andersen [52] thermostat and Berendsen [53] barostat were used for temperature and pressure control, respectively. Ewald [31] summation was used for all non-bonded interactions.

Ball-and-stick and space-filling (CPK) representations of the smaller amorphous cell (one 80-RU chain) are shown in Figure 13-13. Results of simulation values of density for amorphous cells of two different sizes are shown in Table 13-11. As shown, equilibrium values of density appear to be achieved within 250-ps dynamics. The difference in densities between the small cell (23.9 Å on a side) and large cell (30.0 Å on a side) is only about 2% while the computational time for the larger cell is about twice that for the smaller cell. The density of the larger cell averaged over the final 250 ps of NPT dynamics is 1.023 g cm⁻³ (s.d. = 0.007). This value is in reasonable agreement with experimental densities of amorphous PS that have been reported in the range between 1.04 and 1.065 g cm⁻³ [5]. It is possible that using a larger amorphous cell will give even better agreement with experimental data although computational time will significantly increase.

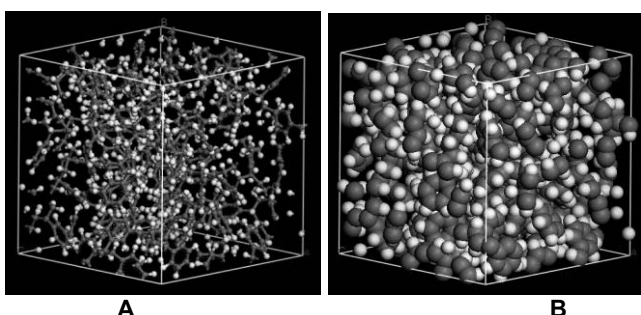


Figure 13-13 Amorphous cell of single PS chain after 500-ps NPT dynamics. **A.** Ball-and-stick representation; **B.** CPK (space-filling) representation (carbon atoms are shown as dark gray spheres).

Table 13–11 Average Densities Obtained from NPT Dynamics of PS Amorphous Cells at 25°C

Avg. Density (g cm ⁻³)	25-ps NPT	250-ps NPT	500-ps NPT
Avg. (s.d.), one chain (80-RU)	0.985 (0.008)	1.001 (0.009)	1.001 (0.009) ^a
Avg. (s.d.), two chains (80-RU)	0.974 (0.007)	1.015 (0.018)	1.023 (0.007) ^b

13.5.2 Cohesive Energy Density and the Solubility Parameter

Cohesive energy density (CED) is another property that can be obtained from MD simulations and used to calculate the solubility parameter (see Sections 3.2.6 and 13.1.4) of a simple liquid or a polymer. Specifically, the CED is obtained by subtracting the average (i.e., intramolecular) energies of the individual molecules in an amorphous cell from the average energy of the total cell and then dividing by the cell volume. The heat of vaporization (ΔH_{vap}) from this energy difference between that of a periodic cell, E_{cell} , and the summation of the energy of the individual molecules, E_i , in the cell is expressed by the equation

$$\Delta H_{\text{vap}} = \left\langle E_{\text{cell}} - \sum_{i=1}^n E_i \right\rangle_p + RT \quad (13.48)$$

where R is the ideal gas constant. Energies are summed over the total number of molecules in the system, n . The brackets indicate that the difference between E_{cell} and E_i is averaged for all ensembles at constant pressure. This average is the *cohesive energy* (E^{coh}). The ΔH_{vap} obtained from simulation on the basis of eq. (13.48) can be compared to the experimental value for small molecules as a method of validating the force field.

The solubility parameter, δ , can be calculated from E^{coh} using the following:

$$\delta = \sqrt{E^{\text{coh}}} = \sqrt{\frac{E}{V}}. \quad (13.49)$$

In this way, simulation provides the opportunity to obtain solubility parameters for polymers for which (1) experimental values are not available and (2) group contributions cannot be used due to the absence of the required group-contribution parameters. As a further validation of the force field, solubility parameters obtained from molecular simulations can be compared with both experimental values (Section 3.2.6) and/or values obtained from group-contribution methods (Section 13.1.4) or topological indices (Section 13.2). As an illustration, the solubility parameter obtained for the larger amorphous cell of polystyrene in Example 13.7 is determined

from simulation to be $13.6 \text{ (J/cm}^3\text{)}^{1/2}$ (s.d. = 0.035) or $13.6 \text{ MPa}^{1/2}$ (averaged over the final 250 ps of NPT dynamics). Experimental values fall within the range of 15.6 to $21.1 \text{ (MPa)}^{1/2}$ [5].

13.5.3 Glass-Transition Temperature

Since density can be obtained from NPT dynamics as described in the previous section, densities obtained at different temperatures and a fixed pressure can be plotted as a function of temperature to obtain the glass-transition temperature (T_g), in a similar fashion to the experimental technique of dilatometry (Section 4.3.2). Values of specific volume ($1/\rho$) calculated from NPT densities obtained for a polyphosphazene (see Section 2.4.2) are plotted against temperature in Figure 13-14. In this example, the T_g corresponding to the intersection of lines obtained from least-square fit of simulation data above and below the T_g is 212 K compared to 198 K from DSC measurements. The use of simulations to determine T_g have been reported for a variety of polymers including polyphosphazenes [54], polysilanes [55], polyethylene [56], polypropylene [56], polyisobutylene [56], polydimethylsiloxane [56], polyoxymethylene [56], and poly(L-lactide) [57] using a variety of force fields. In general, T_g values obtained from NPT dynamics are very similar to values obtained from DSC measurements as shown in Table 13-12.

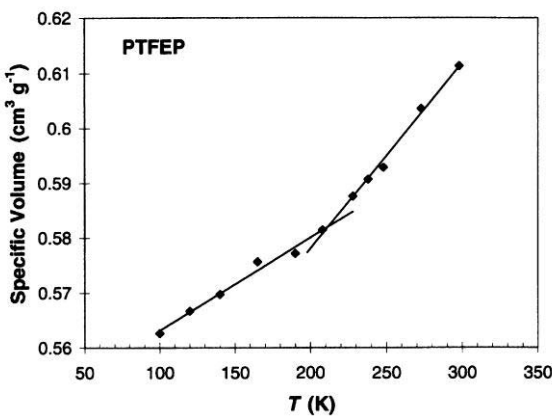


Figure 13-14 Plot of specific volume of a polyphosphazene, poly[bis(2,2,2-trifluoroethoxy)phosphazene], against temperature. As shown by the intersection of the two lines, the T_g is 212 K compared to 198 K from DSC results. Reproduced from J. R. Fried and P. Ren, *Molecular Simulation of Polyphosphazenes. Computational and Theoretical Polymer Science*, 1999, 9: p. 111–166.

Like dilatometry, NPT dynamics can be very time-consuming to get a statistically sufficient number of data points. Advantages of this approach are that T_g can be obtained for synthetic polymers that decompose at temperatures below T_g and for polymers that have not yet been synthesized. As an additional benefit, thermal-expansion coefficients (α) above and below T_g can be obtained from these plots. In addition, comparison between simulated and experimental values of T_g can be used as a validation of the molecular force field selected for the simulation.

Table 13-12 Comparison of Experimental Density and T_g for a Variety of Different Polymers with Values Obtained from NPT Dynamics

Polymer	Density (g cm^{-3})		T_g (K)		Ref.
	Exp.	Sim.	Exp.	Sim.	
Poly[bis(<i>n</i> -butoxy)phosphazene]	1.047	1.005	165	162	[54]
Poly[bis(<i>iso</i> -butoxy)phosphazene]	1.055	1.016	178	178	[54]
Poly[bis(<i>sec</i> -butoxy)phosphazene]	1.104	1.077	182	159	[54]
Poly[bis(2,2,2-trifluoroethoxy)phosphazene]	1.71 ^a	1.633 ^b	198	212 ^b	[54]
Poly(di- <i>n</i> -hexylsilane)	0.971	0.955	221	213	[55]
Poly(propylmethylsilane)	1.047	1.051	245	223–273	[55]
Poly(trifluoropropylmethylsilane)	0.913	0.917	270	266–290	[55]
Polyethylene	0.85	0.868	155, 252	178 ^b	[56]
Polyisobutylene	0.88	0.872	200	192	[56]
Polypropylene	0.85	0.767	259	248 ^b	[56]
Polydimethylsiloxane	0.98	0.995	150, 146	181	[56]
Polyoxymethylene	1.25	1.312	190	191 ^b	[56]

^a 60% crystallinity.

^b amorphous.

13.5.4 Pair Correlations

The pair-correlation function (PCF) or radial distribution function (RDF), $g(r)$, is an extremely useful tool for structural analysis and can provide important information concerning molecular packing, ordering behavior, compressibility, and phase transitions. The PCF can be obtained from experimental studies (e.g., neutron scattering) but also can be conveniently obtained from MD simulations. Plots of specific PCFs, such as the intramolecular and intermolecular PCF between oxygen and hydrogen atoms in water versus atomic distance obtained from simulations, can be directly compared to those obtained from experimental data. Such a comparison provides an excellent basis to validate a force field for a particular system.

Pair-correlation functions provide spherically averaged distributions of interatomic vector lengths. A three-dimensional Fourier transform of the PCF will give the *structure factor* from which X-ray, neutron, and electron diffraction distributions can be predicted and compared with experimental data. In the X-ray diffraction pattern, the first peak in the intermolecular part of the PCF between skeletal atoms gives a direct measure of the average distance between chain backbones in the amorphous bulk.

Calculations can include all the atoms in the model or they can be restricted to comparisons between atoms in two selected groups. The atom pairs included in the calculations can also be restructured to specific elements or force field types. This allows the calculation of the structure factor for each atom in the model; each can then be weighed appropriately before making comparisons with X-ray diffraction data. Calculations can be done using trajectory file data or the coordinates of the current model; however, the trajectory file data allow averaging over multiple frames giving statistically more reliable results.

An example of an application of the insight that PCF calculations can provide is the nature of interactions of CO₂ with fluorinated polymers. This results in high selectivity for CO₂ membrane separations. One polymer that has been considered for this application is poly[bis(2,2,2-trifluoroethoxy)phosphazene] (PTFEP), mentioned in the previous section, whose repeat unit structure is shown in Figure 13-15. The PCFs between CO₂ and the backbone atoms of P and N and with O, CH₂, and CF₃ of the trifluoroethoxy-substituent group of PTFEP were determined using the COMPASS force field parameterized for phosphazenes [37]. In this study [58], PCFs were calculated from an amorphous cell containing four CO₂ molecules and a single chain of 120 repeat units and equilibrated with 2-ns NVT dynamics followed by 1.5-ns NPT dynamics. The PCF was calculated from the relationship

$$g_i(r) = \frac{N_i(r)}{\rho_i N_{\text{CO}_2} N_S 4\pi r^2 dr} \quad (13.50)$$

where $N_i(r)$ represents the number of atoms of type i in a spherical shell contained between r and $r + dr$, ρ_i is the bulk density of atoms of type i in PTFEP, N_S is the total number of frames used for the analysis, and N_{CO_2} is the number of CO₂ molecules. As shown, there is a strong peak near 4.3 Å representing an interaction between CO₂ and CF₃. At greater distances, the PCF reaches a limiting value of unity. These results were shown to agree very closely with the conclusions obtained from *ab initio* computational chemistry calculations of CO₂ with trifluoroethane as a model compound. This comparison provides a very good validation of molecular simulation methods.

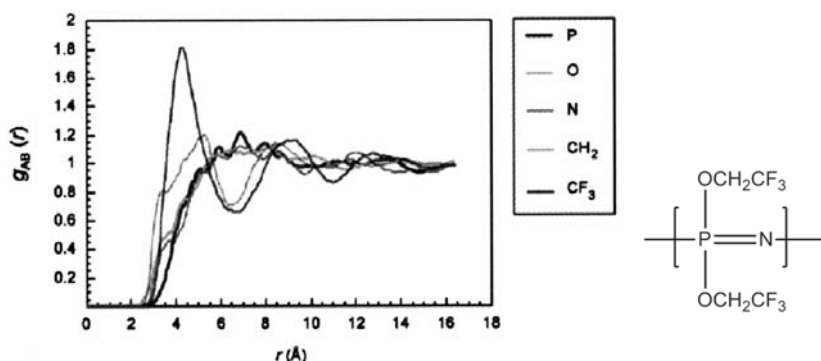


Figure 13-15 Plot of the pair-correlation function, $g_{AB}(r)$, versus the separation distance, $r(\text{\AA})$, between CO_2 and the phosphorus and nitrogen atoms along the chain backbone and between CO_2 and the oxygen atoms, methylene groups of the trifluoroethoxy side chains of poly[bis(2,2,2-trifluoroethoxy)phosphazene] (PTFEP). Reproduced from J. R. Fried and N. Hu, *The Molecular Basis of CO_2 Interaction with Polymers Containing Fluorinated Groups; Computational Chemistry of Model Compounds and Molecular Simulation of Poly[bis(2,2,2,-trifluoroethoxy)-phosphazene]*. Polymer, 2003. **44:** p. 4363–4372.

13.5.5 Time-Correlation Coefficients

One advantage of molecular dynamics over Monte Carlo methods is the ability to calculate time-dependent properties in the form of time-correlation coefficients. An important example is the *velocity autocorrelation function* (VACF) defined as

$$C(m) = \frac{1}{n} \sum_{i=1}^N v(m+1)v(i) \quad (13.51)$$

where m is the maximum number of points allowed for the VACF calculation, n is the number of data points used for averaging, and i is the step counter (i.e., increment). A Fourier transform of the VACF gives the power spectrum useful for predicting vibrational properties such as thermal effects on IR or Raman spectra. The VAC also can be used to determine the self-diffusion coefficient as shown in Section 13.5.5.

Another time-correlation function is the *vectorial* or orientational autocorrelation function defined as [59]

$$m(t) = \langle \mathbf{u}(0) \cdot \mathbf{u}(t) \rangle \quad (13.52)$$

where $\mathbf{u}(t)$ is a vector characterizing the orientation of a polymer backbone or side chain at a given time, t . Using polyphosphazene as a further example, a main-chain vector was defined as one originating from the phosphorus $P(i)$ atom at position i along the backbone to the adjacent nitrogen atom, $N(i+1)$ in the sequence $P(i)-N(i)-P(i+1)-N(i+1)$. In Figure 13-16, the main-chain vectorial autocorrelation functions are plotted versus time for three polyphosphazenes—poly[bis(*n*-butoxy)phosphazene] ($PnBuP$), poly[bis(*iso*-butoxy)phosphazene] ($PiBuP$), and poly[bis(*sec*-butoxy)phosphazene] ($PsBuP$). A value of unity for the vectorial autocorrelation function indicates a totally rigid backbone chain while decreasing values indicate increasing flexibility. As shown, the most sterically hindered side chains result in the highest backbone rigidity as reflected by the following order of decreasing rigidity: $PiBuP > PsBuP > PnBuP$.

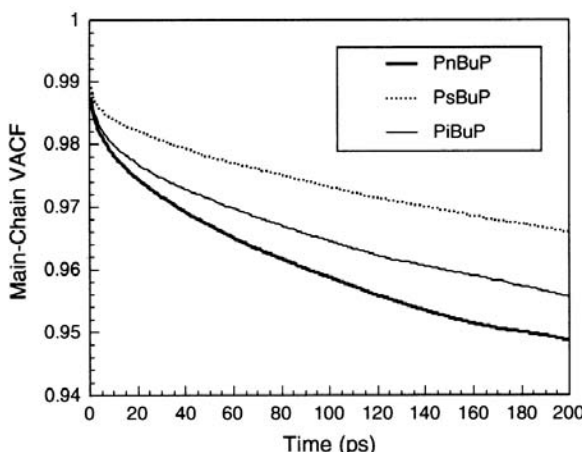


Figure 13-16 Plot of the vectorial autocorrelation function of the backbone chains of three polyphosphazenes over 200 ps of NPT dynamics. Reproduced from J. R. Fried, *Gas Diffusion and Solubility in Poly(organophosphazenes): Results of Molecular Simulation Studies*. Journal of Inorganic and Organometallic Polymers and Materials, 2006, **16**(4): p. 407–418. Copyright 2006 Springer-Verlag.

An additional example of a time-correlation function is the time-dependent *dipole moment*

$$\mu_{\text{tot}}(t) = \sum_{i=1}^N \mu_i(t) \quad (13.53)$$

where $\mu_i(t)$ is the dipole moment of molecule i at time t . The total dipolar correlation function is given by

$$C_{\text{dipole}}(t) = \frac{\langle \mu_{\text{tot}}(t) \cdot \mu_{\text{tot}}(0) \rangle}{\langle \mu_{\text{tot}}(0) \cdot \mu_{\text{tot}}(0) \rangle}. \quad (13.54)$$

The infrared spectra can be obtained from molecular dynamics using a Fourier transform of the dipolar correlation function.

13.5.6 Scattering Functions

Molecular dynamics simulations may be used to reproduce X-ray and neutron scattering spectra that can be compared with experimental data as a test of the validation of the chosen force field for the polymer under study. The intersegmental or d -spacing, an approximate measure of free volume in amorphous polymers, can be obtained from the simulated diffraction patterns through use of the Bragg equation in the form

$$d = \frac{\lambda}{2 \sin \theta} \quad (13.55)$$

where λ is the wavelength (1.5418 Å for CuK α radiation) and θ is the scattering angle corresponding to the maximum of the principal peak in a plot of intensity versus the scattering angle, 2θ . As an illustration, the X-ray diffraction pattern of the high-free-volume polymer, poly[1-(trimethylsilyl)-1-propyne] (PTMSP), is shown in Figure 13-17. As discussed elsewhere [61], the simulated X-ray diffraction pattern and the calculated d -spacing of 9.31 Å agree well with published experimental data.

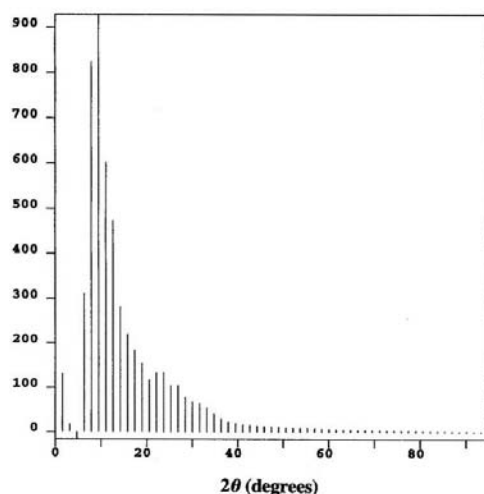


Figure 13-17 Simulated X-ray diffraction pattern of PTMSP. Reproduced from J. R. Fried and D. K. Goyal, *Molecular Simulation of Gas Transport in Poly[1-(trimethylsilyl)-1-Propyne]*. Journal of Polymer Science: Part B: Polymer Physics, 1998. **36**: p. 519–536.

13.5.7 Mechanical Properties

Early developments in the use of atomistic modeling to determine mechanical properties have been reported by a number of groups [62–64]. During simulation of an amorphous cell under externally applied stress, pressure and stress may be controlled using the Parrinello–Rahman algorithm [65], which allows both the shape and volume of the cell to change, thereby enabling the internal stress of the system to match the externally applied stress.

The fundamental relationship between the stress (τ) and strain (ϵ) tensors is given by the generalized Hooke's law in the form

$$\boldsymbol{\tau} = \mathbf{C}\boldsymbol{\epsilon}. \quad (13.56)$$

Since both tensors are symmetric, eq. (13.56) can be written in vector notation as

$$\tau_i = C_{ij}\epsilon_j \quad (13.57)$$

where τ_i and ϵ_j are the six components of the stress and strain vectors, respectively, and C_{ij} is the symmetric 6×6 stiffened matrix. In all there are 21 coefficients to fully describe the stress-strain behavior. For totally isotropic material, only two inde-

pendent coefficients—the Lamé constants, λ and μ —can fully describe the stress-strain behavior. These constants are contained in components of the stiffness matrix for an isotropic material, C_{ij} , as

$$\mathbf{C}_{\text{isotropic}} = \begin{pmatrix} \lambda + 2\mu & \lambda & \lambda & 0 & 0 & 0 \\ \lambda & \lambda + 2\mu & \lambda & 0 & 0 & 0 \\ \lambda & \lambda & \lambda + 2\mu & 0 & 0 & 0 \\ 0 & 0 & 0 & \mu & 0 & 0 \\ 0 & 0 & 0 & 0 & \mu & 0 \\ 0 & 0 & 0 & 0 & 0 & \mu \end{pmatrix}. \quad (13.58)$$

The internal stress is obtained from the first derivative of the potential energy with respect to strain and the diagonal and off-diagonal components of the stiffness matrix are obtained from the second derivative of the potential energy as follows:

$$C_{ii} = \frac{1}{V} \frac{\partial^2 U}{\partial \varepsilon_i^2} \quad (13.59)$$

and

$$C_{ij} = \frac{1}{V} \frac{\partial^2 U}{\partial \varepsilon_i \partial \varepsilon_j} = \frac{\partial \sigma_i}{\partial \varepsilon_j}. \quad (13.60)$$

The Lamé constants can be used to determine Young's modulus (E), bulk modulus (B), shear modulus (G), and Poisson's ratio (ν) through the following relationships:

$$E = \frac{3\lambda + 2\mu}{\lambda/\mu + 1} \quad (13.61)$$

$$\nu = \frac{\lambda}{2(\lambda + \mu)} \quad (13.62)$$

$$B = \lambda + \frac{2\mu}{3} \quad (13.63)$$

and

$$G = \mu. \quad (13.64)$$

In the case of an *anisotropic* material such as a crystal, all coefficients of the stiffness matrix are needed.

13.5.8 Sorption Isotherms

Sorption isotherms of solutes in polymers can be obtained at different pressures by a variety of methods including the Grand Canonical Monte Carlo (GCMC) simulations (μ , T , p). This approach uses a Metropolis [28] algorithm for accepting or rejecting configurational moves (i.e., rotation and translation of the sorbate molecule) as well as for sorbate insertion and deletion. GCMC simulations have been used to predict gas adsorption in zeolites [66] but also can be conveniently used to determine sorption isotherms for polymers. In order to accommodate larger gas penetrants such as CH_4 and CO_2 , amorphous cells of at least 40 Å are recommended to achieve a statistically representative distribution of free-volume sites [67].

In GCMC simulation, the first step is a random selection and insertion of a sorbate molecule into a simulation box. The decision whether to translate or reorient the sorbate molecule is based upon the potential energy of the new configuration. Specifically, the decision to accept or reject the move or return to the original configuration is based upon the probability

$$p_{\text{move}} = \min \left[\exp(-\Delta U/kT); 1 \right] \quad (13.65)$$

where ΔU is the difference in potential energy between the old and new configurations. The decision to accept or reject the new configuration is based on comparing p_{move} with a random number between 0 and 1. The decision to add or subtract is based upon a similar calculation of a probability. For example, the probability for addition can be written as

$$p_{\text{add}} = \min \left[\frac{1}{(N+1)} \frac{pV}{kT} \exp(-\Delta U/kT); 1 \right] \quad (13.66)$$

where N is the number of molecules before the addition, p is the pressure of the bulk gas, and V is the volume of the cell. Such calculations may be performed as many as 10 million times at each pressure before an equilibrium state (i.e., a single point on the sorption isotherm) is reached.

Solubility coefficients can be obtained from the limiting slope of the GCMC sorption isotherms for each gas at low pressure as

$$S = \lim_{p \rightarrow \infty} (C/p) \quad (13.67)$$

where C is the concentration of sorbed gas and p is pressure. In simulation, concentration is reported as the number of sorbate molecules that are sorbed per volume of the simulation cell (\AA^3) at a given pressure (or fugacity). Typical units of experimental solubility coefficients are $\text{cm}^3(\text{STP})/\text{cm}^3$ polymer and, therefore, a unit conversion must be made to compare with experimental data. As an example, sorption isotherms of methane in PTMSP at four temperatures are shown in Figure 13.18. Using eq. (13.67), solubility coefficients were obtained and used to calculate the heat of sorption, ΔH_s , from the van't Hoff expression

$$S = S_0 \exp(-\Delta H_s/RT). \quad (13.68)$$

The simulation value was $-3.08 \text{ kcal mol}^{-1}$, which is in very good agreement with the experimental value of $-3.3 \text{ kcal mol}^{-1}$. Example 13.8 illustrates the use of GCMC calculations to determine the sorption isotherm of O_2 in the rubbery polymer poly-dimethylsiloxane.

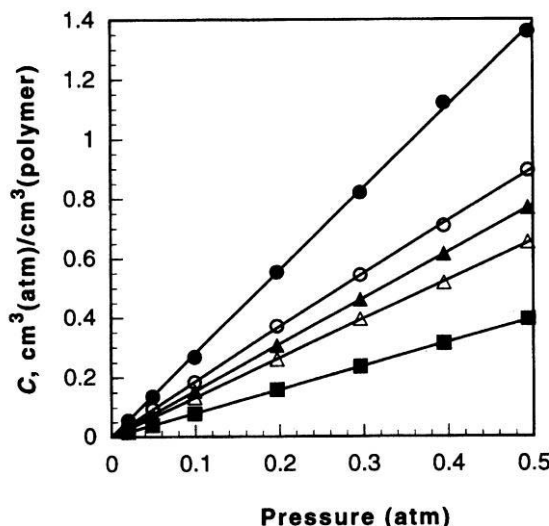


Figure 13-18 Sorption isotherms for CH_4 in PTMSP obtained at 308 K (●), 320 K (▲), 360 K (▲) and 400 K (■). Curves represent dual-mode model fit of simulation data (see Section 12.1.3). Reproduced from T. Zheng and J. R. Fried, *Monte Carlo Simulation of the Sorption of Pure and Mixed Alkanes in Poly[1-(trimethylsilyl)-1-Propyne]*, Separation Science and Technology, 2001. 36(5&6), 959–973.

Example 13.8

Using GCMC simulations, calculate the sorption isotherm of O₂ in polydimethylsiloxane (PDMS) at 298 K.

Solution

For this simulation, the COMPASS [36] force field has been selected. An amorphous cell was built using four PDMS chains each containing 80 repeat units (RUs) at 298 K and an initial density of 0.8 g cm⁻³. The cell was then equilibrated using 25-ps NVT dynamics (Andersen [52] thermostat) at 298 K followed by sequential 250-ps NPT dynamics (Andersen thermostat and Berendsen [53] barostat). Average temperature over 250-ps NPT was 298.0 K. Temperature and density over the final 50 ps of NPT dynamics was 297.8 (s.d. = 2.8) K and 1.0170 g cm⁻³ (s.d. = 0.0063). The final amorphous cell at the end of the 250-ps NPT dynamics was 36.5 Å on a side. This structure was used for the O₂ sorption measurements at 298 K from 10 to 1000 total fugacity using GCMC (configurational bias^{*}). Because PDMS is a rubbery polymer ($T_g = 120$ K), the sorption isotherm is linear ($R^2 = 0.9993$) as shown in Figure 13-19.

Experimentally determined densities of silicone rubber fall within the range around 0.97 to 0.98 g cm⁻³. Silicone rubber is not pure PDMS but is lightly crosslinked and may contain some fillers or additives; however, the simulation density of 1.0170 g cm⁻³ is less than 5% higher than reported experimental values. The experimental solubility coefficient obtained from the O₂ isotherm using eq. (13.67) for O₂ has been reported [68] to be 0.18(± 0.01) cm³(STP)/cm³ polymer atm at 35°C. Reported simulation values have been in the range from 0.22 to 0.25 cm³(STP)/cm³ polymer atm in reasonable agreement with the GCMC results in this example. The solubility units refer to the volume (cm³) of the gas (O₂) at standard temperature and pressure (i.e., 273 K, 1 bar) while cm³ polymer is the unit of volume of the experimental polymer sample used in the sorption measurements.

* In configurational bias, the solute is inserted into the amorphous cell using different orientations. This is important for accurate simulation of the sorption of asymmetric molecules such as ethanol.

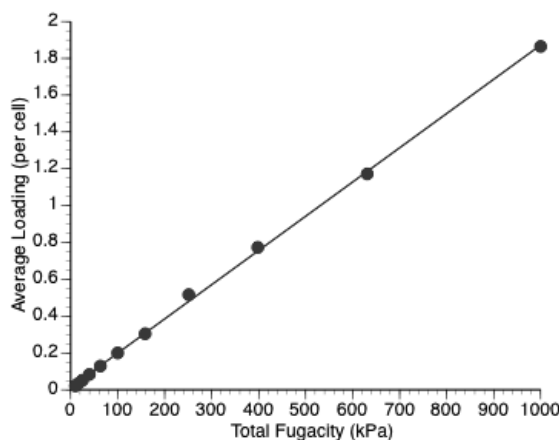


Figure 13-19 Sorption isotherm of O₂ in PDMS at 298 K obtained by GCMC simulation at 298 K. Line represents a least-square fit of the data points.

The slope of the simulated isotherm shown in Figure 13-19 is 1.859×10^{-3} molecules per cell/kPa. To compare with the experimental results, we need to convert from molecules per cell/kPa to the experimental units of cm³(STP)/cm³ polymer atm. This requires several steps. First, the molar volume of an ideal gas at STP is 0.02245 m³ or 2.242×10^4 cm³. Second, the volume of the amorphous cell is calculated as $(36.5 \text{ \AA})^3 = 48,630 \text{ \AA}^3 = 4.87 \times 10^{-20}$ cm³. The final conversion is given as

$$\frac{1.86 \times 10^{-3} \text{ molecules}}{\text{kPa}} \frac{\text{kPa}}{9.87 \times 10^{-3} \text{ atm}} \frac{9.87 \times 10^{-3} \text{ atm}}{4.87 \times 10^{-20} \text{ cm}^3 \text{ polymer}} \frac{4.87 \times 10^{-20} \text{ cm}^3 \text{ polymer}}{2.24 \times 10^4 \text{ cm}^3(\text{STP})} \times \frac{2.24 \times 10^4 \text{ cm}^3(\text{STP})}{\text{mol}} \times \frac{\text{mol}}{6.02 \times 10^{23} \text{ molecules}} = \frac{41.7}{289.4} = 0.144 \frac{\text{cm}^3(\text{STP})}{\text{cm}^3 \text{ polymer atm}}.$$

The value of $0.144 \text{ cm}^3(\text{STP})/\text{cm}^3 \text{ polymer atm}$ obtained at 298 K compares well with reported experimental values of 0.18 and $0.224 \text{ cm}^3(\text{STP})/\text{cm}^3 \text{ polymer atm}$ and other simulation values of 0.22 and $0.25 \text{ cm}^3(\text{STP})/\text{cm}^3 \text{ polymer atm}$.

13.5.9 Permeability

The permeability coefficient (P) is the product of the diffusion coefficient (D) and the solubility coefficient (S). Both can be obtained from molecular simulations including the use of MD and MC simulations as discussed in the following sections.

Diffusion Coefficients. The self-displacement coefficient, D , can be obtained from MD simulations, typically NVT or NVE dynamics, through two approaches. The most frequently used is the Einstein relationship

$$D_\alpha = \frac{1}{6N_\alpha} \lim_{t \rightarrow \infty} \frac{d}{dt} \left\langle \sum_i^N |\mathbf{r}_i(t) - \mathbf{r}_i(0)|^2 \right\rangle \quad (13.69)$$

where N_α is the number of diffusing species. The term in brackets is the mean-square displacement (MSD) where $\mathbf{r}_i(t)$ is a vector representing the final position of particle i (atom or molecule) at time t and $\mathbf{r}_i(0)$ is the initial position at the start of the dynamics. Equation (13.69) applies in the region of Einstein diffusion where $n = 1$ in the following relationship between the MSD and time:

$$\left\langle |\mathbf{r}_i(t) - \mathbf{r}_i(0)|^2 \right\rangle \propto t^n. \quad (13.70)$$

For very short times, the MSD may be quadratic in time (i.e., $n = 2$) characteristic of “free flight” as may occur in a pore or cage well. In the processing of simulation data, the MSD is plotted as a function of elapsed time and D is calculated as 1/6 of the slope of the best-fit line. Typically, the initial trajectories, where $n = 2$, are discarded from the data used to calculate D . In addition, the MSD versus time plot is typically noisy near the end of the simulation due to the way that trajectories are averaged and, therefore, these data points are also excluded when D is calculated.

An example of a log–log plot of MSD versus time for O₂ and CO₂ diffusing in an amorphous cell of the high-free-volume glassy polymer poly[1-(trimethylsilyl)-1-propyne] (PTMSP) (see Section 12.1.2) is shown in Figure 13-20. The plot shows that Einstein diffusion is reached by 32 ps in this case. Diffusion coefficients at 300 K obtained using a customized DREIDING [32] force field and MSD data in the Einstein region were found to be 2.38×10^{-5} cm² s⁻¹ for O₂ in good agreement with the experimental value. Procedures for calculating O₂ diffusion in the highly permeable rubbery polymer polydimethylsiloxane (PDMS) are shown next in Example 13.9.

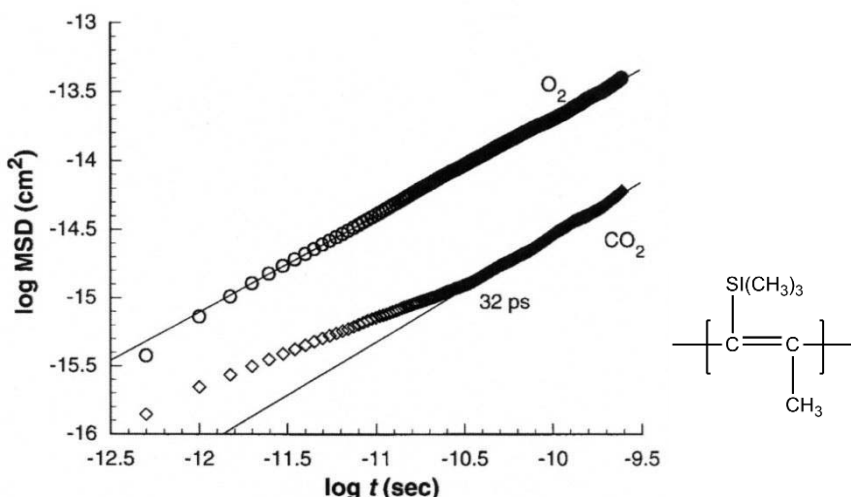


Figure 13-20 Log–log plot of MSD versus NVT simulation time for oxygen and carbon dioxide in poly[1-(trimethylsilyl)-1-propyne] (PTMSP). Reproduced from J. R. Fried and D. K. Goyal, *Molecular Simulation of Gas Transport in Poly[1-(trimethylsilyl)-1-Propyne]*. Journal of Polymer Science: Part B: Polymer Physics, 1998. **36**: p. 519–536. Reprinted by permission of John Wiley, Inc.

An alternative approach makes use of the velocity autocorrelation function (VACF) given by the Green–Kubo relation as

$$D = \frac{1}{3} \int \mathbf{v}(t) \cdot \mathbf{v}(0) dt \quad (13.71)$$

where $\mathbf{v}_i(t)$ is the center-of-mass velocity vector of a single molecule at time t . In general, MD simulations can be expected to provide meaningful estimates of the diffusion coefficient for rapid diffusion (i.e., $>10^{-8}$ to 10^{-7} cm s⁻¹). In the case of slower diffusion, such as the investigation of diffusion in barrier polymers, an alternative approach using atomistic simulations is the transition state theory (TST) of Suter and Gusev [69].

Example 13.9

Using MD solutions, calculate the diffusion coefficient of O₂ (O=O) in polydimethylsiloxane (PDMS) at 298 K.

Solution

Using the COMPASS force field, an amorphous cell was constructed using the same procedures as used in Example 13.8 except four oxygen molecules were built into the cell. As before, 25-ps NVT and 250-ps NPT dynamics were used to equilibrate the cell. The final density at the end of 250-ps NPT dynamics was 1.026 g cm^{-3} at 292.8 K. The amorphous cell, shown in Figure 13-21, was 36.4 \AA on a side (density of 1.026 g cm^{-3}). Figure 13-21 shows the four oxygen molecules (in space-filling representation) in the box containing the PDMS chains shown as line representations. Next, 1.0-ns NVT dynamics were used to obtain trajectories to determine the diffusion coefficient. Average temperature during the 1.0-ns NVT dynamics was 298.4 K (s.d. = 3.2) with an average pressure of 0.017 GPa (s.d. = 0.084 GPa).

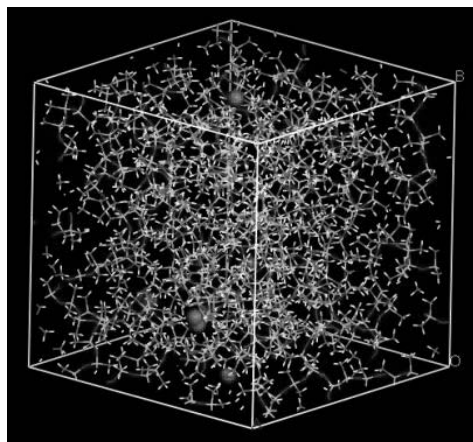


Figure 13-21 Amorphous cell of PDMS containing four O_2 molecules (CPK space-filling representation).

The MSD plot is shown Figure 13-22. As shown in Figure 13-23, a log–log plot of MSD versus time shows reasonable linearity between 125 and 625 ps (slope = 0.95, $R^2 = 0.9988$). The good linearity with a slope of the log–log plot near unity is a good indication that diffusion is within the Einstein region. The slope in the plot of MSD versus time (ps) over this time range gives a slope of $0.7065 \text{ \AA}^2/\text{ps}$ ($R^2 = 0.9974$). The diffusion coefficient at 298 K is then calculated from eq. (13.69) as

$$D = \frac{\text{slope}}{6} = \frac{0.7065 \text{ \AA}^2}{6 \text{ ps}} \frac{(10^{-8}) \text{ cm}^2}{\text{\AA}^2} \frac{\text{ps}}{10^{-12} \text{ s}} = 0.1178 \times 10^{-4} \frac{\text{cm}^2}{\text{s}} = 11.8 \times 10^{-6} \frac{\text{cm}^2}{\text{s}}$$

The value of $11.8 \times 10^{-6} \text{ cm}^2 \text{ s}^{-1}$ obtained here compares well with experimental values reported in the range from 16 to $41 \times 10^{-6} \text{ cm}^2 \text{ s}^{-1}$ at temperatures up to 308 K. Other simulation studies reported in the literature give diffusion coefficients for O_2 in the range from 4.5 to $35 \times 10^{-6} \text{ cm}^2 \text{ s}^{-1}$.

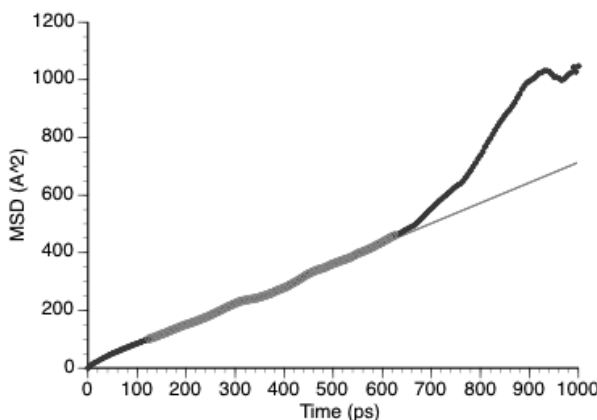


Figure 13-22 Plot of MSD versus NVT simulation time for O₂ in PDMS. Data used in the calculation of the diffusion coefficient are indicated in red. The thin line shown is the least-square fit of that data.

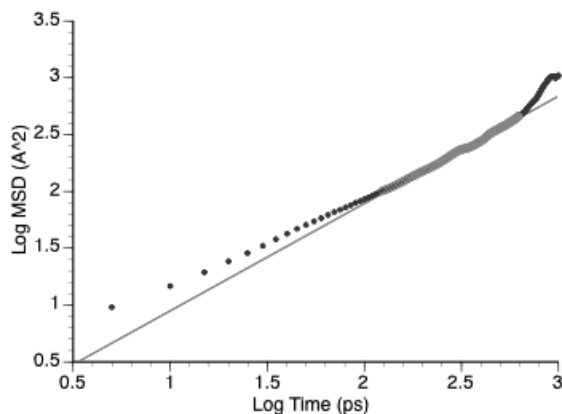


Figure 13-23 Log–log plot of MSD versus NVT simulation time for O₂ in PDMS.

Solubility Coefficients. The solubility coefficient, S , can be obtained from several approaches such as the calculation of excess chemical potential, μ_{ex} , as

$$S = \exp(-\mu_{\text{ex}}/RT) \quad (13.72)$$

where μ_{ex} is obtained from the calculated interaction energy, E , from the Widom insertion method (1963). Alternatively, the solubility coefficient can be obtained from the sorption isotherm obtained using GCMC simulation (Section 13.5.8) from eq. (13.67).

Permeability Coefficients. Once the diffusion and solubility coefficients have been determined from simulation, the permeability coefficient can be estimated as

$$P = DS. \quad (13.73)$$

Using the values of S and D for O_2 in PDMS (Examples 13.7 and 13.8), the permeability coefficient can be estimated as*

$$\begin{aligned} P(O_2) &= \left(11.8 \times 10^{-6} \frac{\text{cm}^2}{\text{s}} \right) 0.144 \frac{\text{cm}^3(\text{STP})}{\text{cm}^3(\text{polymer}) \text{ atm}} = \\ &1.70 \times 10^{-6} \frac{\text{cm}^3(\text{STP})}{\text{cm}(\text{polymer}) \text{ atm s}} \frac{1 \text{ atm}}{76 \text{ cm Hg}} = \\ &2.24 \times 10^{-8} \frac{\text{cm}^3(\text{STP}) \text{ cm}}{\text{cm}^2(\text{polymer}) \text{ s cm Hg}} = 224 \text{ Barrer.} \end{aligned} \quad (13.74)$$

Considering the errors associated with the simulation of diffusion and particularly solubility using small atomistic cells, this value of 224 Barrer obtained entirely from simulation reasonably compares with values of around 933 Barrer cited for the O_2 permeability of PDMS [70].

13.5.10 Free Volume

Free volume and free-volume distribution control such important properties as gas diffusivity as described previously. Free volume can be obtained from simulation by a variety of methods including geometric methods such as the Voronoi and Delaunay tessellations of space [71, 72], the Voorinthonk method [73] that utilizes the van der Waals surface of the polymer chain to determine free volume, the TST method mentioned in the previous section, the phantom bubble method [74], and a more recent approach by Sanchez [75].

Voronoi tessellation produces a distribution of polyhedrals using a procedure that bisects the vectors connecting one atom to all other atoms by a plane perpendicular to itself. A related tessellation procedure is called the Delaunay tessellation whereby all contiguous pairs of atoms (i.e., those whose polyhedrals have a com-

* $1 \text{ Barrer} = \frac{10^{-10} \text{ cm}^3(\text{STP}) \text{ cm}}{\text{cm}^2 \text{ s cmHg}}.$

mon face) are joined. A schematic representation of Voronoi and Delaunay tessellation in two dimensions is shown in Figure 13-24.

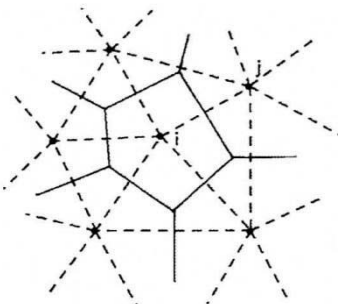


Figure 13-24 Two-dimensional representation of a Voronoi polygon around atom i . The network formed by the dashed lines is the result of the Delaunay tessellation. Reproduced from S. Arizzi, P. H. Mott, and U. W. Suter, *Space Available to Small Diffusants in Polymeric Glasses: Analysis of Unoccupied Space and Its Connectivity*. Journal of Polymer Science: Part B: Polymer Physics, 1992. **30**: 415–426. Reprinted by permission of John Wiley & Sons, Inc.

SUGGESTED READING

- Bicerano, J., *Prediction of Polymer Properties*. 3rd ed. 2002, New York: Marcel Dekker, Inc.
- Binder, K., *Monte Carlo and Molecular Dynamics Simulations in Polymer Science*. 1995, New York: Oxford University Press.
- Fried, J. R., *Molecular Simulation of Gas and Vapor Transport in Highly Permeable Polymers*, in *Materials Science of Membranes for Gas and Vapor Separation*, B. D. Freeman, I. Pinna, and Y. Yampolskii, eds. 2006, London: John Wiley & Sons. p. 94.
- Fried, J. R., *Computational Chemistry and Molecular Simulations*. 2014, New York: John Wiley & Sons.
- Kremer, K., *Computer Simulations for Macromolecular Science*. Macromolecular Chemistry and Physics, 2003. **204**: p. 247.
- Müller-Plathé, F., *Permeation of Polymer—A Computational Approach*. Acta Polymerica, 1994. **45**: p. 259–293.
- Rigby, D., and B. E. Eichinger, *Polymer Modeling*. Current Opinion in Solid State Material Science, 2001. **5**: p. 445.
- Sumpter, B. G., D. W. Noid, and B. Wunderlich, *Computer Simulation and Modeling of Polymer Crystal*. Trends of Polymer Science, 1993. **1**(6): p. 160.

- Theodorou, D. N., *Principles of Molecular Simulation of Gas Transport in Polymers*, in *Materials Science of Membranes for Gas and Vapor Separation*, B. D. Freeman, I. Pinna, and Y. Yampolskii, eds. 2006, London: John Wiley & Sons, p. 49.
- van Krevelen, D. W., *Group Contribution Techniques for Correlating Polymer Properties and Chemical Structure*, in *Computational Modeling of Polymers*, J. Bicerano, ed. 1992, New York: Marcel Dekker, Inc., p. 55.
- Voth, G. A., ed. *Coarse-Graining of Condensed Phase and Biomolecular Systems*. 2009, CRC Press: Boca Raton.

PROBLEMS

13.1 Poly(2,6-dimethyl-1,4-phenylene oxide) (PDMPO) can be partially crystallized in solution (i.e., solvent-induced crystallization). **(a)** Calculate the density of 100% crystalline PDMPO using the group-contribution parameters given in Table 13-1. **(b)** If the crystallinity of a semicrystalline sample of PDMPO is 8%, estimate its crystallinity using the relationship

$$V_{sc} = x_c V_c + (1 - x_c) V_a$$

where x_c is the degree of crystallinity, V_c is the molar specific volume of a 100% crystalline polymer, and V_a is the molar specific volume of the totally amorphous polymer.

13.2 Using the values of molar attraction constants given by van Krevelen in Table 13-2, calculate the solubility parameters, units of $(\text{MPa})^{1/2}$, at 25°C of the following polymers whose densities are given within parentheses:

- (a)** Polyisobutylene ($\rho = 0.924 \text{ g cm}^{-3}$)
(b) Polystyrene ($\rho = 1.04 \text{ g cm}^{-3}$)
(c) Polycarbonate ($\rho = 1.20 \text{ g cm}^{-3}$)

13.3 Using UNIFAC-FV, estimate the activity of toluene in a 50 wt% solution of polydimethylsiloxane in toluene at 298 K.

13.4 Based upon their calculated Permachors, order the following polymers in terms of their expected performance as oxygen barriers: **(a)** amorphous Teflon, **(b)** polyisobutylene, **(c)** polychloroprene, **(d)** polybutadiene, **(e)** nitrile rubber, **(f)** silicone rubber, and **(g)** butyl rubber. Does your result give the correct order based upon experimental permeability values?

REFERENCES

1. Poling, B. E., J. M. Prausnitz, and J. P. O'Connell, *The Properties of Gases and Liquids*. 5th ed. 2001, New York: McGraw-Hill Book Company.
2. van Krevelen, D. W., *Properties of Polymers*. 3rd ed. 1990, Amsterdam: Elsevier.

3. van Krevelen, D. W., *Group Contribution Techniques for Correlating Polymer Properties and Chemical Structure*, in *Computational Modeling of Polymers*, J. Bicerano, ed. 1992, New York: Marcel Dekker, Inc. p. 55–123.
4. Bicerano, J., *Prediction of Polymer Properties*. 3rd ed. 2002, New York: Marcel Dekker, Inc.
5. Mark, J. E., ed., *Polymer Data Handbook*. 2nd ed. 2009, Oxford: Oxford University Press.
6. Bondi, A., *Physical Properties of Molecular Crystals*. 1968, New York: John Wiley & Sons.
7. Thran, A., G. Kroll, and F. Faupel, *Correlation Between Fractional Free Volume and Diffusivity of Gas Molecules in Glassy Polymers*. *Journal of Polymer Science: Part B: Polymer Physics*, 1999. **37**: p. 3344–3358.
8. Fried, J. R., *Correlative Techniques for the Estimation of the Glass-Transition Temperature*. *Computational Polymer Science*, 1993. **3**: p. 47–58.
9. Salame, M., *Transport Properties of Nitrile Polymers*. *Journal of Polymer Science, Polymer Symposium*, 1973. **41**: p. 1–15.
10. Salame, M., *Prediction of Gas Barrier Properties of High Polymers*. *Polymer Engineering and Science*, 1986. **26**(22): p. 1543–1546.
11. Stern, S. A., V. M. Shah, and B. J. Hardy, *Structure-Permeability Relationships in Silicone Polymers*. *Journal of Polymer Science: Part B: Polymer Physics*, 1987. **25**: p. 1263–1298.
12. Small, P. A., *Some Factors Affecting the Solubility of Polymers*. *Journal of Applied Chemistry*, 1953. **3**: p. 71–80.
13. Hoy, K. L., *New Values of the Solubility Parameters from Vapor Pressure Data*. *Journal of Paint Technology*, 1970. **42**: p. 76–118.
14. Barton, A. F. M., *CRC Handbook of Polymer-Liquid Parameters and Solubility Parameters*. 1990, Boca Raton: CRC Press.
15. Brandrup, J., E. H. Immergut, and E. A. Grulke, eds. *Polymer Handbook*. 4th ed. 1999, New York: John Wiley & Sons..
16. Fried, J. R., J. S. Jiang, and E. Yeh, *Group-Contribution Methods in Polymer Thermo-dynamics*. *Computational Polymer Science*, 1992. **2**: p. 95–113.
17. Oishi, T., and J. M. Prausnitz, *Estimation of Solvent Activities in Polymer Solutions Using a Group-Contribution Method*. *Industrial Engineering Chemical Process Design and Development*, 1978. **17**: p. 333–339.
18. Fredenslund, A., R. L. Jones, and J. M. Prausnitz, *Group-Contribution Estimation of Activity Coefficients in Nonideal Liquid Mixtures*. *AIChE Journal*, 1975. **21**(6): p. 1086–1592.
19. Abrams, D. S. and J. M. Prausnitz, *Statistical Thermodynamics of Liquid Mixtures: A New Expression for the Excess Gibbs Energy of Partly or Completely Miscible Systems*. *AIChE Journal*, 1975. **21**(1): p. 116–128.
20. Derr, E. L., and C. H. Deal, *Predicted Compositions during Mixed Solvent Evaporation from Resin Solutions Using the Analytical Solution of Groups Method*, in *Advances in Chemistry Series*, R. W. Tess, ed., 1973, ACS:Washington DC, vol 124, p. 11–30.
21. Hansen, H. K., et al., *Vapor-Liquid Equilibria by UNIFAC Group Contributions. 5. Revision and Extension*. *Industrial and Engineering Chemistry and Research*, 1991. **30**: p. 2352–2355.
22. Bicerano, J., *Prediction of the Properties of Polymers from Their Structures*. *Journal of Macromolecular Science—Reviews in Macromolecular Chemistry and Physics*, 1996. **C36**(1): p. 161–196.
23. Sumpter, B. G., and D. W. Noid, *Neural Networks and Graph Theory as Computational Tools for Predicting Polymer Properties*. *Macromolecular Theory and Simulation*, 1994. **3**: p. 363–378.
24. Liu, W., and C. Cao, *Artificial Neural Network Prediction of Glass Transition Temperature of Polymers*. *Colloid and Polymer Science*, 2009. **287**: p. 811–818.

25. Nielsen, S. O., et al., *Coarse Grain Models and the Computer Simulation of Soft Material*. Journal of Physics: Condensed Matter, 2004. **16**: p. R481–R512.
26. Girard, S., and F. Müller-Plathe, *Coarse-Graining in Polymer Simulations*. Lecture Notes in Physics, 2004. **640**: p. 327–356.
27. Voth, G. A., ed., *Coarse-Graining of Condensed Phase and Biomolecular Systems*. 2009, Boca Raton: CRC Press.
28. Metropolis, N., et al., *Equation of State Calculations by Fast Computing Machines*. Journal of Chemical Physics, 1953. **21**(6): p. 1087–1092.
29. Christen, M., and W. F. van Gunsteren, *Multigraining: An Algorithm for Simultaneous Fine-Grained and Coarse-Grained Simulation of Molecular Systems*. Journal of Chemical Physics, 2006. **124**: p. 1541061.
30. Dinur, U., and A. T. Hagler, *New Approaches to Empirical Force Fields*, in *Reviews in Computational Chemistry*, K. B. Lipkowitz and B. D. Boyd, eds. 1991, New York: VCH Publishers, Inc. p. 99–164.
31. Ewald, P., *Die Berechnung Optischer und Elektrostatischer Gitterpotentiale*. Annals of Physics, 1921. **64**: p. 253–287.
32. Mayo, S. L., B. D. Olafson, and W. A. Goddard III, *DREIDING: A Generic Force Field for Molecular Simulations*. Journal of Physical Chemistry, 1990. **94**: p. 8897–8909.
33. Fried, J. R., *Computational Parameters*, in *Physical Properties of Polymers Handbook*, J. E. Mark, ed. 2007, Springer. p. 59–65.
34. Scott, W. R. P., et al., *The GROMOS Biomolecular Simulation Program Package*. Journal of Physical Chemistry, 1999. **103**: p. 3596–3607.
35. Hwang, M. J., T. P. Stockfisch, and A. T. Hagler, *Derivation of Class II Force Fields. 2. Derivation and Characterization of a Class II Force Field, CFF03, for the Alkyl Functional Groups and Alkane Molecules*. Journal of the American Chemical Society, 1994. **117**: p. 2515–2525.
36. Sun, H., *COMPASS: An Ab Initio Force-Field Optimized for Condensed-Phase Applications—Overview with Details on Alkane and Benzene Compounds*. Journal of Physical Chemistry B, 1998. **102**: p. 7338–7364.
37. Sun, H., P. Ren, and J. R. Fried, *The COMPASS Force Field: Parameterization and Validation for Phosphazenes*. Computational and Theoretical Polymer Science, 1998. **8**(1/2): p. 229–246.
38. Blaisten-Barojas, E., and M. R. Nyden, *Molecular Dynamics Study of the Depolymerization Reactions in Simple Polymers*. Chemical Physics Letters, 1990. **A205**: p. 499–505.
39. Nyden, M. R., and D. W. Noid, *Molecular Dynamics of Initial Events in the Thermal Degradation of Polymers*. Journal of Physical Chemistry, 1991. **95**(2): p. 940–945.
40. van Duin, A. C. T., et al., *ReaxFF: A Reactive Force Field for Hydrocarbons*. Journal of Physical Chemistry A, 2001. **105**: p. 9396–9409.
41. Chenoweth, K., et al., *Simulations on the Thermal Decomposition of a Poly(dimethyl-siloxane) Polymer Using the ReaxFF Reactive Force Field*. Journal of the American Chemical Society, 2005. **127**: p. 7192–7202.
42. Marrink, S. J., et al., *The MARTINI Force Field*, in *Coarse-Graining of Condensed Phase and Biomolecular Systems*, G. A. Voth, ed. 2009, Boca Raton: CRC Press, p. 5–39.
43. Marrink, S. J., et al., *The MARTINI Force Field: Coarse Grained Model for Biomolecular Simulations*. Journal of Physical Chemistry B, 2007. **111**: p. 7812–7824.
44. Marrink, S. J., A. H. de Vries, and A. E. Mark, *Coarse Grained Model for Semiquantitative Lipid Simulations*. Journal of Physical Chemistry B, 2004. **108**: p. 750–760.
45. Shinoda, W., R. Devane, and N.L. Klein, *Multi-Property Fitting and Parameterization of a Coarse-Grained Model for Aqueous Surfactants*. Molecular Simulation, 2007. **33**: p. 27–36.

46. Verlet, L., *Computer “Experiments” on Classical Fluids. I. Thermodynamical Properties of Lennard-Jones Molecules*. Physical Review, 1967. **159**: p. 98–103.
47. Hockney, R. W., and J. W. Eastwood, *Computer Simulations Using Particles*. 1981, New York: McGraw-Hill.
48. Ryckaert, J.-P., G. Ciccotti, and H. J. C. Berendsen, *Numerical Integration of the Cartesian Equations of Motion of a System with Constraints: Molecular Dynamics of n-Alkanes*. Journal of Computational Physics, 1977. **23**: p. 327–341.
49. Anderson, H. C., *A “Velocity” Version of the Shake Algorithm for Molecular Dynamics Calculations*. Journal of Computational Physics, 1983. **52**: p. 24–34.
50. Nosé, S., *A Unified Formulation of the Constant Temperature Molecular Dynamics Methods*. Journal of Chemical Physics, 1984. **81**(1): p. 511–519.
51. Hoover, W. G., *Canonical Dynamics: Equilibrium Phase-Space Distributions*. Molecular Physics, 1985. **31**(3): p. 1695–1697.
52. Andersen, H. C., *Molecular Dynamics Simulations at Constant Pressure and/or Temperature*. Journal of Chemical Physics, 1980. **72**(4): p. 2384–2383.
53. Berendsen, H. J. C., *Molecular Dynamics with Coupling to an External Bath*. Journal of Chemical Physics, 1984. **81**(8): p. 3684–3690.
54. Fried, J. R., and P. Ren, *Molecular Simulation of the Glass Transition of Polyphosphazenes*. Computational and Theoretical Polymer Science, 1999. **9**: p. 111–116.
55. Fried, J. R., and B. Li, *Atomistic Simulation of the Glass Transition of Di-Substituted Polysilanes*. Computational and Theoretical Polymer Science, 2001. **11**: p. 273–281.
56. Yu, K.-Q., Z.-S. Li, and J. Sun, *Polymer Structures and Glass Transition: A Molecular Dynamics Simulation Study*. Macromolecular Theory and Simulation, 2001. **10**(6): p. 624–653.
57. Zhang, J., et al., *Study of the Molecular Weight Dependence of Glass Transition Temperature for Amorphous Poly(L-lactide) by Molecular Dynamics Simulation*. Polymer, 2007. **48**: p. 4900–4905.
58. Fried, J. R. and N. Hu, *The Molecular Basis of CO₂ Interaction with Polymers Containing Fluorinated Groups; Computational Chemistry of Model Compounds and Molecular Simulation of Poly[bis(2,2,2-trifluoroethoxy)phosphazene]*. Polymer, 2003. **44**: p. 4363–4372.
59. Müller-Plathé, F., *Permeation of Polymer—A Computational Approach*. Acta Polymerica, 1994. **45**: p. 259–293.
60. Fried, J. R., *Gas Diffusion and Solubility in Poly(organophosphaznes): Results of Molecular Simulation Studies*. Journal of Inorganic and Organometallic Polymers and Materials, 2006. **16**(4): p. 407–418.
61. Fried, J. R., and D. K. Goyal, *Molecular Simulation of Gas Transport in Poly[1-(trimethylsilyl)-1-Propyne]*. Journal of Polymer Science: Part B: Polymer Physics, 1998. **36**: p. 519–536.
62. Theodorou, D. H., and U. W. Suter, *Atomistic Modeling of Mechanical Properties of Polymeric Glasses*. Macromolecules, 1986. **19**: p. 139–154.
63. Brown, D., and J. H. R. Clarke, *Molecular Dynamics Simulation of an Amorphous Polymer under Tension. I. Phenomenology*. Macromolecules, 1991. **24**: p. 2075–2082.
64. Rutledge, G. C., and U. W. Suter, *Calculation of Mechanical Properties of Poly(p-Phenylene terephthalamide) by Atomistic Modelling*. Polymer, 1991. **32**(12): p. 2179–2189.
65. Parrinello, M., and A. Rahman, *Strain Fluctuations and Elastic Constants*. Journal of Chemical Physics, 1982. **76**: p. 2662–2666.
66. Razmus, D. M., and C. K. Hall, *Prediction of Gas Adsorption in 5A Zeolites Using Monte Carlo Simulation*. AIChE Journal, 1991. **37**(5): p. 769–779.

67. Cuthbert, T. R., N. J. Wagner, and M.E. Paulaitis, *Molecular Simulation of Glassy Polystyrene: Size Effects on Gas Solubilities*. Macromolecules, 1997. **30**: p. 3058–3065.
68. Merkel, T. C., et al., *Gas Sorption, Diffusion, and Permeation in Poly(dimethylsiloxane)*. Journal of Polymer Science: Part B: Polymer Physics, 2000. **38**: p. 415–434.
69. Gusev, A. A., and U. W. Suter, *Dynamics of Small Molecules in Dense Polymer Subject to Thermal Motion*. Journal of Chemical Physics, 1993. **99**: p. 2228–2234.
70. Stern, A. A., V. M. Shah, and B. J. Hardy, *Structure-Permeability Relationships in Silicone Polymers*. Journal of Polymer Science: Polymer Physics Edition, 1987. **25**: p. 1263–1298.
71. Brostow, W., J.-P. Dussault, and B. L. Fox, *Construction of Voronoi Polyhedra*. Journal of Computational Chemistry, 1978. **29**: p. 81–92.
72. Tanemura, M., T. Ogawa, and N. Ogita, *A New Algorithm for Three-Dimensional Voronoi Tesselation*. Journal of Computational Physics, 1983. **51**: p. 191–207.
73. Voorintholt, R., et al., *A Very Fast Program for Visualizing Protein Surfaces, Channels and Cavities*. Journal of Molecular Graphics, 1989. **7**: p. 243–245.
74. Lee, S., and W. L. Mattice, *A Phantom Bubble Model for the Distribution of Free Volume in Polymers*. Computational and Theoretical Polymer Science, 1999. **9**: p. 57–61.
75. in't Veld, P. J., et al., *Liquid Structure via Cavity Size Distributions*. Journal of Physical Chemistry B, 2000. **104**: p. 12028–12034.
76. Arizzi, S., P. H. Mott, and U. W. Suter, *Space Available to Small Diffusants in Polymeric Glasses: Analysis of Unoccupied Space and Its Connectivity*. Journal of Polymer Science: Part B: Polymer Physics, 1992. **30**: p. 415–426.